CHALMERS
UNIVERSITY OF TECHNOLOGY

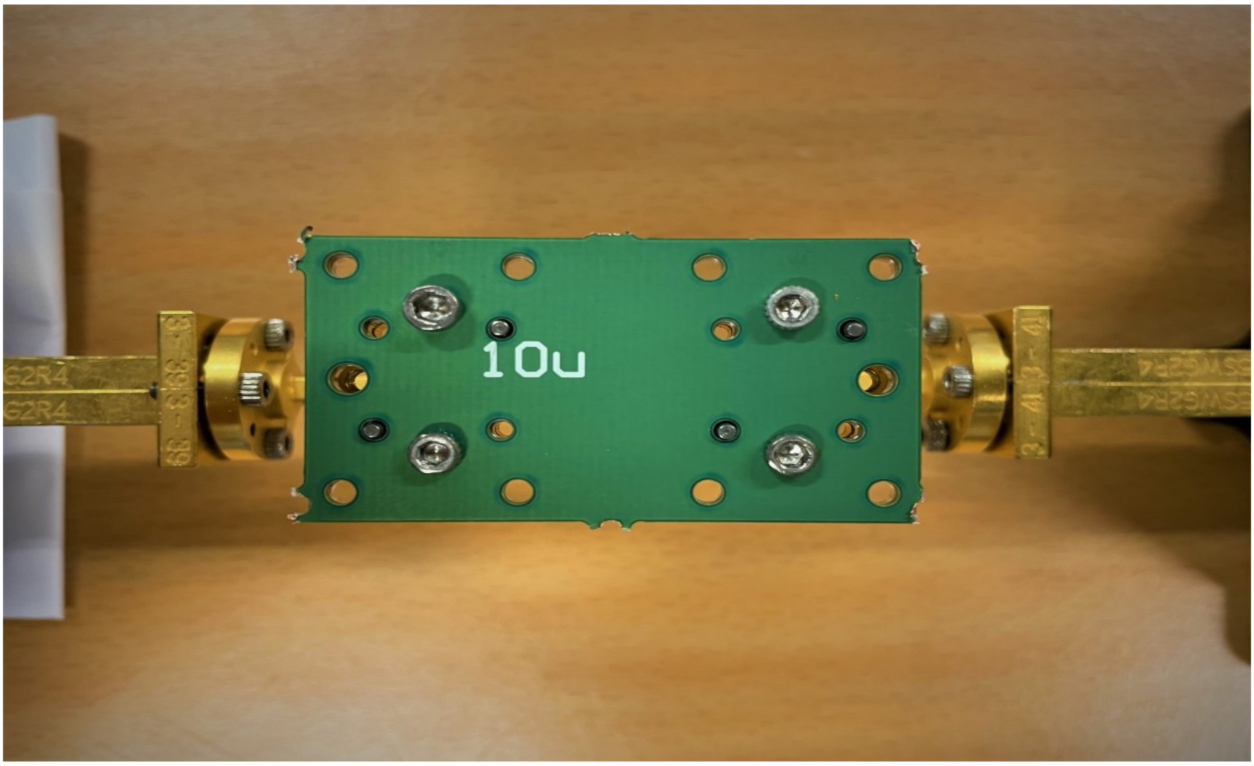

Microstrip-to-Waveguide transition for 140 GHz using Gap waveguide technology

A transition design from an RF circuit to a 140 GHz for multiple applications along with different matching techniques for optimum results

Master's thesis in Wireless, Photonics and Space Engineering

ANISH MISHRA

Department of Electrical Engineering
CHALMERS UNIVERSITY OF TECHNOLOGY
Gothenburg, Sweden 2021
www.chalmers.se

MASTER'S THESIS 2021

Microstrip-to-Waveguide transition for 140 GHz using Gap waveguide technology

A transition design from an RF circuit to a 140 GHz for multiple applications along with different matching techniques for optimum results

ANISH MISHRA

Department of Electronics Engineering
Division of Communication Antenna and Optical Networks
CHALMERS UNIVERSITY OF TECHNOLOGY
Gothenburg, Sweden 2021

Microstrip-to-Waveguide transition for 140 GHz using Gap waveguide technology
A transition design from an RF circuit to a 140 GHz for multiple applications along with different matching techniques
for optimum results
ANISH MISHRA

© ANISH MISHRA, 2021.

Supervisor: Hanna Karlsson, GapWaves AB
Supervisor: Qiannan Ren, Department of Electrical Engineering
Examiner: Ashraf Uz Zaman, Department of Electrical Engineering

Master's Thesis 2021
Department of Electrical Engineering
Antenna Systems
Chalmers University of Technology
SE-412 96 Gothenburg
Telephone +46 31 772 1000

Cover: Measurement setup for testing the fabricated design

Typeset in LaTeX
Printed by Chalmers Reproservice
Gothenburg, Sweden 2021

Microstrip-to-Waveguide transition for 140 GHz using Gap waveguide technology
A transition design from an RF circuit to a 140 GHz for multiple applications along with different matching techniques
for optimum results
Anish Mishra
Department of Electrical Engineering
Chalmers University of Technology

Abstract

The increasing demand in data rates have already exploited mmWave technology that has been implemented in 5G along with higher bandwidth and transmit power for automotive radar applications. However, there is a further necessity of higher bit rates and miniaturization of components for various integration applications. The D-band (110-170GHz) seems to be the next generation technology that can fulfill the industrial expectations.

In this master thesis, various microstrip to gap waveguide transition designs at 140GHz has been discussed along with the manufacturing and evaluation of optimal designs. Different matching techniques have been implemented for tolerance performance analysis. There are transitions available for E-band technology used in automotive radar applications (76-81GHz). However, the system becomes more sensitive and susceptible to misalignment's between the difference stages of the transition design limiting its flexibility in terms of fabrications. Dielectric material properties changes with increase in frequency that affects conventional performance mentioned by the manufacturers.

The testing of the transition is done using Ridge Gap waveguide technology where back-to-back structures have been manufactured to ease the process of verifying the results. Multiple variants of transitions has been designed to test the robustness and compensate for error during the manufacturing process. The prototype provides with the expected bandwidth of 15-25GHZ for both quarterwave and stub matching fabricated PCBs. The insertion loss for both quarterwave and stub matching is less than 1.15dB for the working bandwidth of the transitions. Similarly, the return loss is greater than 10dB for both quarterwave and stub matching within the range of working bandwidth.
Keywords: Gap Waveguide, Transition, Substrate, Ridge Waveguide, D-band.

Acknowledgements

This work has been carried out in collaboration with Chalmers University of Technology and Gapwaves AB.

Firstly, I would like to thank my mentor, Antenna Engineer, Hanna Karlsson, for her guidance and valuable support throughout the master thesis. She was there to guide me during each step and I really appreciate all her efforts to get the best out of my project. It was a different scenario with the pandemic situation but everyone at GapWaves AB were supportive and proactive during various stages of the thesis. Furthermore, I would like to thank Qiannan Ren for taking the time to assist and discuss ideas during the whole process and provide his valuable time during the measurements. Finally, I am pleased for all the expertise and support from professor Ashraf Uz Zaman through out the project and giving me an opportunity to be a part of this remarkable Master's thesis.

I would also like to appreciate all the support from my friends who joined during Erasmus and motivated me to work hard during the pandemic which was one of the major driving factor. The excitement from my hometown friends to finish my Master's degree pushed my motivation further ahead to defend my master thesis at the earliest.

My mother has always been supportive and thanks to all of her courage during the tough times which allowed me to pursue my Master's. Thanks to my little sister who took care of things back at home due to which I was able to focus on my studies. At the end, I will like to dedicate this thesis to my father who always dreamed of this day but sadly could not witness this moment. I hope his blessings are always with me and he is proud of this moment as we together achieved this milestone.

Anish Mishra, Gothenburg, August 2021

Contents

List of Figures

List of Tables

1
Introduction

1.1 Background

The trend for increasingly higher frequencies continues for integrated millimeter wave (mm-wave) radar systems. The motivation for these mm-wave radar systems is inspired by the market competition to provide more features at low costs which includes enhanced RF functionality, minimal chip area, low power dissipation and higher digital reconfigurability. Modern cars have already implemented radar systems to measure the radial distance and velocity of surrounding objects very precisely. The environmental conditions such as fluctuations in temperature, bad lighting due to various weather conditions does not affect the performance of this technology.

The 24 GHz and 77 GHz are the two primary frequency band which has been extensively used for automotive radars. The sensor size reduces as we move higher in frequency which makes the overall system compacts due to which 77 GHz radars are in demand and implemented widely in recent years. The 77 GHz provides smaller antenna size compared to 24 GHz for a given beamwidth requirement along with good angular resolution for a small sensor size [1]. The industry keeps on innovating various features to improve the functionality of the cars and hence there is always a requirement if the systems could be made more compact and efficient altogether. Artificial Intelligence (AI) and Machine Learning (ML) is enforced on automotive industries which has made it possible for the cars to become completely autonomous. There is a need of ultra high resolution radar sensors for automotive application that will provide high precision along with enough data for processing and improving the systems.

W-band and D-band are the next available bands while moving up in the frequency spectrum that can provide us with massive amounts of additional bandwidth and higher data rate that can certainly be a part of the solution[2]. Another advantage of D-band is that we can achieve higher antenna gain with the same size of antenna that is used for lower frequency applications. The European CEPT Electronic Communications Committee (ECC) issued recommendation 18(01) in 2018, where more than 30GHz of sub-bands over the D-band frequencies were allocated for fixed service backhaul and fronthaul [3]. These recommendations encouraged the industries to develop components and technologies that will support these high speed wireless link network. The D-band could be a promising technology for backhaul as it provides higher beamwidth and higher energy efficiency[4].

1.2 This work

The purpose of this master thesis is to design a microstrip to waveguide transition from RF circuit to slot array antennas for D-band applications using gap waveguide technologies. The thesis includes several parts which explains working of different type of gap waveguides structures and complete design journey of the final transition product. The comparison between a H-plane and E-plane transitions based on the simulation result has also been presented along with their advantages and drawbacks over each other for better understanding of the preferred technique. E-plane design was manufactured and implemented with a back-to-back configuration to ease the process of testing at this high frequency.
The tolerance analysis is another important parameter that is the limelight of the master thesis to conclude the complete performance of the design. The simulation is always the ideal case, however in a practical case, the design measurements differs due to the manufacturing process. The substrate performance has been scaled to D-band frequency which would also affect the performance of the design. The transition itself includes two parts that includes the microstrip patch on the substrate and the D-band gap waveguide structure. These two parts should be perfectly aligned in order to get the expected results. As we move up in higher frequency, the components becomes smaller and hence even few changes in *um* would deviate the results which could affect the overall performance of the transition design. Hence, It is necessary to consider all the parameters for tolerance and make sure that the design is capable of handling these tolerances to provide the desired performance.
Back-to-back (B2B) configuration is used to measure the transition design results since it is more flexible to connect the probes at the waveguide openings compared to connecting the probes on the microstrip for such a smaller dimensions with the same accuracy. However, in a future product, single ended configuration is used to feed the signal from a RF circuit to the necessary device (Antennas or Radars). It was out of scope of the thesis to discuss more about the RF circuit and the Antennas/Radars which would be using the designed transition and hence the report is limited with the details about the transition and gap waveguide technology for D-band application.

2

Theory

2.1 Basics of Electromagnetic Radiation

Electromagnetic waves are the combination of electric and magnetic field which are perpendicular to each other and the direction of propagation of the wave. These waves are characterized by a wide range of wavelengths and frequencies, where each is identified with a specific intensity (or amplitude) and quantity of energy. Depending on these varying frequencies, a broad spectrum has been derived with different regions like Radio Frequency (RF), Tera-Hertz (THz), Infra Red (IR), visible, Ultraviolet (UV), gamma radiation, etc along with their applications as shown in the figure 2.1. It can thus be inferred that if there is an existing EM field, it is not enough to form an EM wave or radiation, as this requires some additional conditions. Thus, EM radiation often refers only to states that allow the emission and propagation of EM waves, although the state of EM field can be considered as the state of energy radiation.

Electromagnetic waves can travel through free space which is the ideal form of propagation. However, electromagnetic wave can also be guided through specific media with different material properties which will manipulate the behaviour of the wave. Conductive media like metals forms a barrier that does not allow the radiation to travel through it whereas, signals are attenuated to different levels in some media based on their properties[7].

The Electric field of a uniform plain wave equation with only an x-component propagating in the z direction can be written as follows:

$$E_x(z) = E^+ e^{-jkz} + E^- e^{jkz} \tag{2.1}$$

where E^+ and E^- are the arbitrary wave amplitudes. The -z and +z represents the direction of the propagation where -z denotes the positive direction and +z denotes the negative direction for the propagation of the wave. The $k = \omega\sqrt{\mu\epsilon}$ is the propagation constant where ω is the angular frequency, μ and ϵ are the permittivity and permeability of the dielectric material. The phase velocity in any medium is defined as the rate of propagation of a wave and is denoted as V_p which is given as:

$$V_p = \frac{\omega}{k} \tag{2.2}$$

The λ is the wavelength which is defined as the distance between two successive minima or maxima on the wave at a fixed instant of time [5].

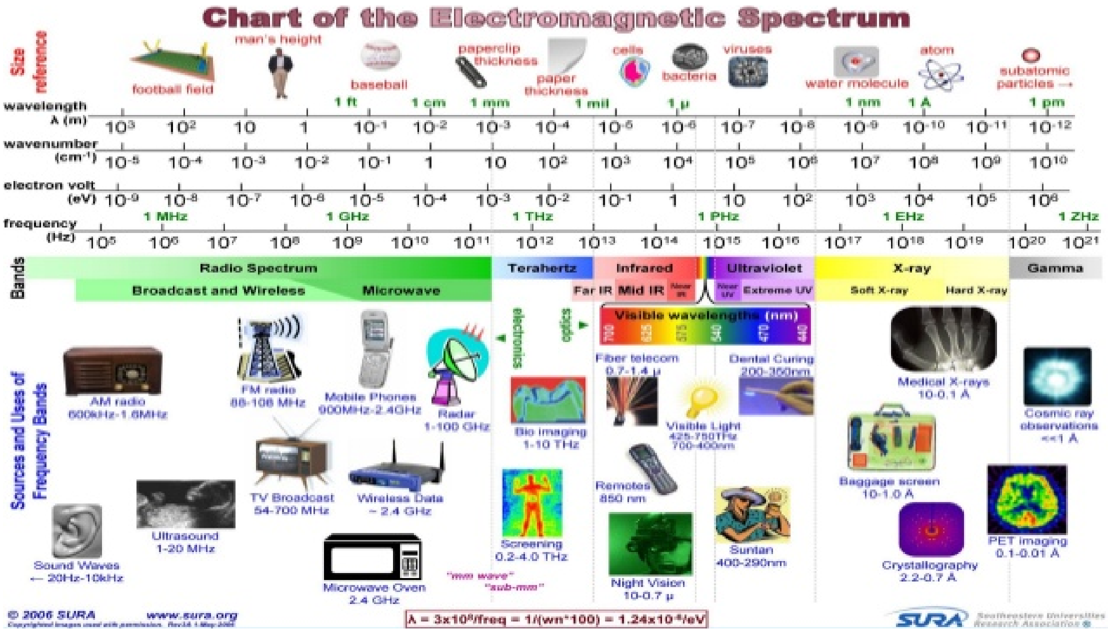

Figure 2.1: Comparison of frequency band designations [6]

2.1.1 Electromagentic Loss Mechanism

The conductive loss α_c, dielectric loss α_d, and losses incurred due to undesired radiation α_r are the main losses that may occur when an electromagnetic wave is propagating in a lossy medium. The attenuation constant α can be approximated as follows:

$$\alpha = \alpha_c + \alpha_d + \alpha_r \tag{2.3}$$

The conductive loss α_c is mainly impacted by the conductivity and roughness of the conducting surface. This could be calculated along the length of the conductor which is given be the equation 2.4. The skin depth δ, which defines the depth of penetration of the propagating electromagnetic waves at higher frequencies decreases.

$$\alpha_c = \frac{R_s}{2Z_0\eta}\frac{\partial Z_0}{\partial l} \tag{2.4}$$

Where R_s is the surface resistivity of the conductor, $\eta = \sqrt{\mu_0/\epsilon}$ is the dielectric's intrinsic impedance. The 2^{nd} term in the equation signifies the characteristic impedance over the complete length of the conductor.

The dielectric loss α_d can be calculated using the propagation constant γ for a line or guide completely filled with homogeneous dielectric and can be given as follows:

$$\alpha_d = \frac{k^2 \tan\delta}{2\beta} \tag{2.5}$$

Where $\tan\delta$ is the loss tangent which determines the losses in the dielectric and β is the phase constant of the electromagnetic wave. The $\tan\delta$ is the material specific property that could be modified in order to reduce the losses.

The final loss deriving α_r from undesired radiation defines the energy that is coupled to any radiating or leaking mode which can be mostly minimized by building a well-designed structure. The above equations are referred from the book "Microwave Engineering" and in-depth details are mentioned in the reference [5].

2.2 Microwave Systems

In the event where the wavelength of the signal approaches towards the dimensions of the electrical components, based on the voltage and current being approximately constant across the component or circuit, classical circuit theory can no longer be applicable. Therefore, it becomes imperative to opt for microwave circuit theory considering the examination of the voltage and the current at the exact phase. This could further lead to the consequence of the impedance concept modifying and becoming more complex as the quantity changes with time and position, which can for the reason be difficult to specify. It may appear to be complex and time-consuming in terms of design and analysis; there are however certain tools developed to simplify the calculations and applied to the most common microwave problems. Below are the two important concepts of microwave circuit theory i.e, Impedance Matching and Scattering Parameters are explained.

2.2.1 Impedance Matching

Components having different impedances are often connected to achieve the desired results, however, due to their different impedances undesired power losses occurs due to reflections . To assure more stability in phase and amplitude with low loss, there is a need to apply impedance matching. Hence, in microwave theory impedance matching holds essential importance. Among the several methods available for impedance matching, two of them will be further explained.

The first method consists of a technique most relevant when there is a desire to create a match between two real-valued impedances, namely the quarter-wave transformer. In its simplest form, at center frequency, the matching network consists of a single section transformer at quarter wavelength. The frequency-dependent length resulting in the narrowband transformer can be expanded using multiple sections for improved bandwidth. In the analysis of the transformer presented in [5], it can be concluded that optimum matching is achieved when the matching section has an impedance Z_1 of

$$Z_1 = \sqrt{Z_0 Z_L} \tag{2.6}$$

where Z_L and Z_0 are the two impedances to match.
The second method is commonly used for the reason that it is easy to apply and is capable of achieving good impedance matching, it is mainly based on using short or open-circuited stubs. The stub contributes with a reactance, whose value is dependent on the electrical length of the stub and whether it is short or open-

circuited. As is the case for the quarter-wave transformer, the reactance depends on the electrical length where the stub is fairly narrowband. However, it is possible to expand the bandwidth by using two or more stubs and simultaneously obtain a more flexible structure with the introduction of more tunable parameters.

2.2.2 Scattering parameters

While dealing with high-frequency networks, voltages and currents are not the ideal quantities for measurements. Microwave frequencies involves magnitude and phase of a travelling wave in a particular direction. It is fairly easier to calculate and define impedances and hence S-parameters became standards for high frequencies applications. S-parameters are combined into a S-matrix which describes the incident and reflected voltages on various port as shown in the equation below:

$$\begin{bmatrix} V_1^- \\ V_2^- \\ \cdots \\ V_N^- \end{bmatrix} = \begin{bmatrix} S_{11} & S_{12} & \cdots & S_{1N} \\ S_{21} & \ddots & & S_{2N} \\ \vdots & \cdots & & \vdots \\ S_{N1} & \cdots & & S_{NN} \end{bmatrix} \begin{bmatrix} V_1^+ \\ V_2^+ \\ \cdots \\ V_N^+ \end{bmatrix} \tag{2.7}$$

The S_{ij} has different properties where S_{11} shows the return loss of the device, S_{21} provides us with the insertion loss and this could be extended further depending on the number of ports. The elements in the matrix can be further determined by:

$$S_{ij} = \left.\frac{V_i^-}{V_j^+}\right|_{V_k^+ = 0 \,\text{for}\, k \neq j} \tag{2.8}$$

From the equation (2.8), we can find all the S_{ij} by the driving port j with an incident wave voltage V_j^+ and measuring the reflected amplitude V_i^- coming out of port i. Except the j^{th} port, all other ports on which the waves are incident are set to zero that means all the ports should be terminated in matched loads to avoid reflections.

We can derive Insertion loss (IL) and return loss(RL) from the S-parameters which are ususally considered for determining the performances of a matching section or transitions between various components. The insertion loss is give as:

$$IL = -20\, log_{10} \left| S_{21} \right| dB \tag{2.9}$$

whereas, the return loss is given as:

$$RL = -20\, log_{10} \left| S_{11} \right| dB \tag{2.10}$$

2.3 Transmission lines and Antennas

Transmission lines are usually considered as two conductors or two wire line and it is generally modeled as a lumped-element circuit as shown in figure 2.2. A segment

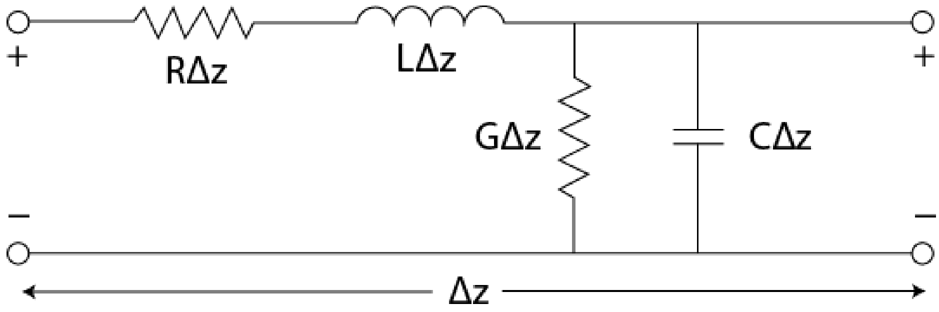

Figure 2.2: Lumped element circuit of a parallel line

of a transmission line modeled with quantities R,L,C and G are specified per unit length where

$$\text{Series resistance along the line} = R$$
$$\text{Series Inductance along the line} = L$$
$$\text{Shunt capacitance along the line} = C$$
$$\text{Shunt Inductance along the line} = G$$

The series resistance R is due to the finite conductivity of the conductors whereas dielecric losses between the conductors due to the material properties is represented by G. The self-inductance of the two conductors is denoted by L and due to the small distance between the two conductors, a capacitance is formed that is denoted by C. All these quantities are depended on the length of the transmission line Δz. The transmission lines can be categorized as follows:

1. Two wire parallel transmission line
2. Coaxial transmission line
3. Strip type transmission line
4. Waveguides

Antenna can be termed as a device to radiate or receive electromagnetic radiation. It couples the electromagnetic radiation between the free space and waveguide, tranmission lines, couplers which are present at the transmitter and/or receiver. Antennas are one of the vital components in wireless communication system as various systems have different requirements and antennas needs to be optimized based on specific applications. Antennas are used in various applications such as mobile communication, space and satellite communication for radio astronomy meteorolgy, military and radar applications, weather and air-traffic radars. The size for antennas varies based on their applications which exhibits different characteristics such as wavelength, power, gain, directivity, beamwidth, etc [8]. The different types of Antennas are as follows:

1. Wire antennas
2. Slot antennas
3. Microstrip antennas
4. Horn antennas
5. Reflector antennas
6. Linear Planar array antennas

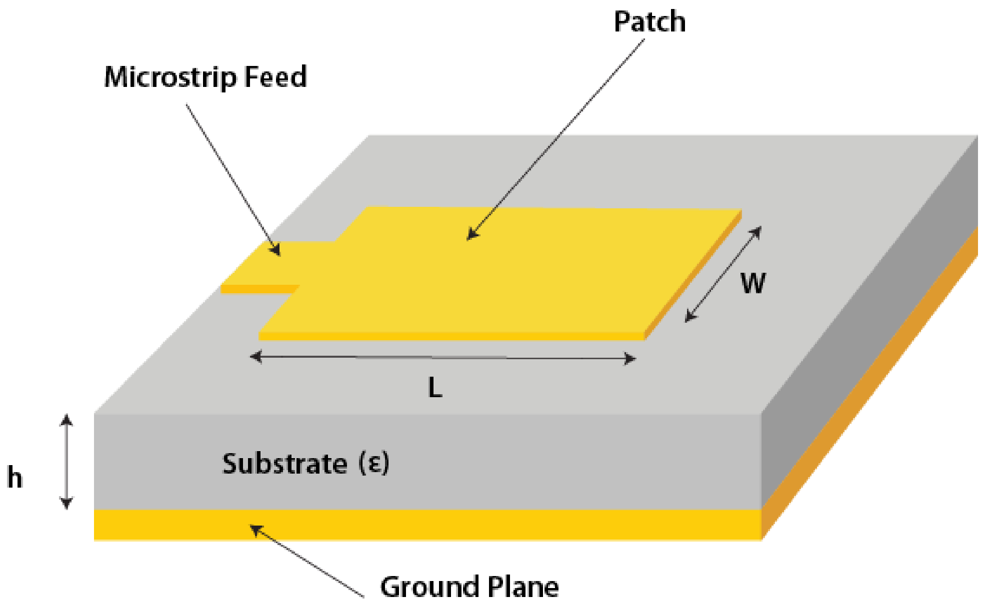

Figure 2.3: An overview of microstrip patch antenna

A brief introduction of microstrip antenna is explained specifically as it will be implied in further sections for the design of transitions. Microstrip antennas are fabricated on a printed circuit board which are usually etched out on a metal film on a dielectric material (substrate). These antennas could be in different forms such as patches, slots or strips and are usually cost effective to manufacture in terms of mass production. As antenna's size varies based on their desired frequency band, these antennas could be made really compact for microwave frequency range with the optimum performance based on the effeciency of the designed antenna.

The radiating patch can be in various shapes like rectangular or circular with slits or tuning stubs for increased bandwidth. These antennas can be excited in multiple ways which include probe feeding through coaxial connectors. Another widely used method for microwave frequencies is directly feeding the patch with a microstrip line which is etched out on the same substrate reducing the need for soldering and connectors minimizing the losses. Figure 2.3 shows the microstrip patch antenna of length (L) and width (W) excited by a microstrip line of width (ω). The thickness of the substrate is given by (h) with a dielectric permittivity (ϵ) of the substrate. The width (W) f the microstrip patch can be calculated with the following equation [8] [9]:

$$W = \frac{c}{2 \times f_r} \times \sqrt{\frac{2}{\epsilon + 1}} \tag{2.11}$$

where f_r is the operating frequency of the antenna c is the speed of light ($3 \times 10^8 m/s$). The effective dielectric constant of a microstrip line is approximately given by:

$$E_{eff} = \frac{E_r + 1}{2} + \frac{E_r - 1}{2} \frac{1}{\sqrt{1 + 12 \times \frac{h}{W}}} \tag{2.12}$$

which could be further used to calculate the L of the microstrip patch as follows:

$$L_{eff} = \frac{\lambda_0}{2 \times \sqrt{E_{eff}}} \tag{2.13}$$

$$\Delta L = 0.412 \times h \times \frac{(E_{eff} + 0.3)}{(E_{eff} - 0.258)} \times \frac{(\frac{W}{h} + 0.264)}{(\frac{W}{h} + 0.8)} \tag{2.14}$$

where L_{eff} is the effective length and ΔL is the fringing fields at the length of the patches. The actual length of the microstrip patch can then be calculated as [8] [9]:

$$L = L_{eff} - 2 \times \Delta L \tag{2.15}$$

For the characteristic impedance of 50Ω, we can calculate the line impedance of the microstrip feed line by the formulas given below:

$$Z_0 = \begin{cases} \frac{60}{\sqrt{E_{eff}}} \ln\left(\frac{8h}{\omega} + \frac{\omega}{4h}\right) & \text{if } \omega/d \leq 1 \\ \frac{120\pi}{\sqrt{E_{eff}}\left[\frac{\omega}{h} + 1.393 + 0.667 \ln\left(\frac{\omega}{d} + 1.444\right)\right]} & \text{if } \omega/d \geq 1 \end{cases} \tag{2.16}$$

Once we have acquired the Z_0 and ϵ we can easily calculate the ratio for ω/h:

$$\frac{\omega}{d} = \begin{cases} \frac{8e^A}{e^{2A} - 2} & \text{if } \omega/d < 2 \\ \frac{2}{\pi}\left[B - 1 - \ln(2B - 1) + \frac{\epsilon - 1}{2\epsilon}\left(ln(B - 1) + 0.39 - \frac{0.61}{\epsilon}\right)\right] & \text{if } \omega/d > 2 \end{cases} \tag{2.17}$$

where

$$A = \frac{Z_0}{60}\sqrt{\frac{\epsilon - 1}{2}} + \frac{\epsilon - 1}{\epsilon + 1}\left(0.23 + \frac{0.11}{\epsilon}\right)$$
$$B = \frac{377\pi}{2Z_0\sqrt{\epsilon}}$$

The characteristic impedance of the microstrip line should be matched with the input impedance of the rectangular patch for minimum losses. The distribution of magnetic field is maximum at the center, white it is minimum on the outer edges of the patch. Whereas, the distribution of electric field is minimum at the center but it is maximum at the edges of the patch. The easiest way to match the line with the patch is to find a point on the radiating surface where the impedance is 50Ω and connect the feed probe to this point. For this work, the radiating patches and matching sections has been referred from the previous work of similar transitions and has been optimized directly. However, the above techniques are useful to calculate precise values for the patch and matching sections.

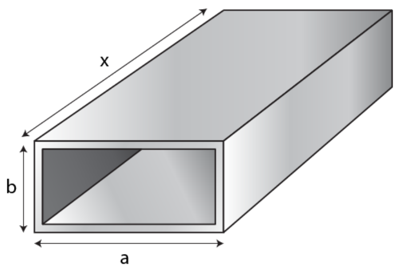

Figure 2.4: Hollow Rectangular Waveguide

2.4 Waveguide

Hollow rectangular waveguides are commonly used waveguide in microwave frequencies applications. These hollow waveguides is applicable to frequencies as low as 300 MHz or several THz which makes them easily available in markets. These waveguide are ideally made of infinite length in x direction and of finite height and width as shown in the figure 2.4. The physical mechanisms are basically the metallic walls or dielectric boundaries and the size and shape of these walls/boundaries will determine the characteristics of the guided modes. Maxwell's equation along with the associated boundary conditions is applicable to determine the existence of the guided modes [12]. The different type of waveguides are as follows:

1. Rectangular waveguide
2. Circular waveguide
3. Elliptical waveguide
4. Single ridged waveguide
5. Double ridged waveguide

The rectangular waveguide can only support Transverse Electric(TE) and Transverse Magnetic(TM) mode of propagation. Due to the presence of only one conductor, there is no propagation of TEM mode. Each waveguide has it's cutt off frequency (f_c) which determines the dominant mode. Below f_c there would be no mode of propagation:

$$f_c = \frac{1}{2\pi\sqrt{\mu\epsilon}}\sqrt{\left(\frac{m\pi}{a}\right)^2 + \left(\frac{n\pi}{b}\right)^2} \tag{2.18}$$

The dominant mode for a rectangular waveguide is TE_{10} which is usually the dominant mode. Parameters a and b are the dimensions of the waveguide which plays a major role in deciding the cutt off frequency of a particular waveguide, whereas m and n are the mode numbers. Parameteres μ and ϵ are the permeability and permittivity of the dielectric material of the waveguide as these waveguides can be filled with dielectric material for specific applications.

2.5 Gap Waveguide Technology

Gap Waveguide technology has gained potential in recent years to become a leading performer in millimeter waveguide applications. The components are based on the bed of nails, a periodic structure composed by metallic pins covered by a metal lid. It is an extension of the research about hard and soft surfaces where hard surfaces have the ability to enhance the propagation and soft surfaces were used to attenuate the propagation or stop waves of any polarization. A gap waveguide could be manufactured with an ideal parallel plate waveguide, where one of the plate is constructed of perfect electric conductor (PEC) and another plate is made of perfect magnetic conductor (PMC). As long as the distance between the two plates is less than $\lambda/4$, no wave can propagate between the plates. However, if we integrate a metal strip to the PMC surface, then we can propagate the EM wave along the strip line.

The bed of nails creates AMC or high impedance surface (HIS) that blocks electromagnetic wave propagation in certain frequency range. These bed of nails depending on their pin dimensions determines the frequency range and could be modified based on the requirements. Waveguides can be created using these structures, where a cavity is formed between the bed of nails that could be used as the baseline to propagate the wave and forbid the wave propagation in all other directions[13].

In reality there are no PMC's available and hence, in practical applications, the PMC condition is emulated by an artifical magnetic conductor (AMC) in the form of periodic metallics structure such as pins or other textured structures. In an actual gap waveguide, there is enough high impedance on the AMC surface to create a stopband over which no parallel-plate modes can propagate. The guiding structures could be in the form of grooves, ridges or strips which will create a virtual wall on both sides of guiding section preventing the lateral field leakage. Following are the different types of gap waveguide technology that are widely used in various applications [13] [14]:

1. Ridge gap waveguide
2. Groove gap waveguide
3. Inverted microstrip gap waveguide

We will focus more on ridge and groove waveguide technology in the next section.

2.5.1 Ridge and Groove Waveguides

The ability to create parallel-plate stopband in the undesired direction for wave propagation is the main characteristic of the gap waveguide technology. Once the stopband is obtained, a guiding ridge or a groove may be integrated in the periodic pin structure to propagate a mode. Incase of a ridge waveguide in figure 2.5, a quasi TEM wave is propagated whereas a mode similar to TE_{10} is obtained in the groove waveguide 2.5. The height between the PEC and the periodic pin structure should be less than $\lambda/4$ to ensure the mode propagation. The figure 2.5 shows the geometries for both ridge and groove gap waveguides.

The working principle of both the waveguides are same except the guiding structure which is either a metal strip (Ridge) or a groove created in the textured surface. The lower and higher frequency cutoff for the pin stop band is dependent on multiple factors. The height and width of the pins (radius in case of cylindrial pins), period of

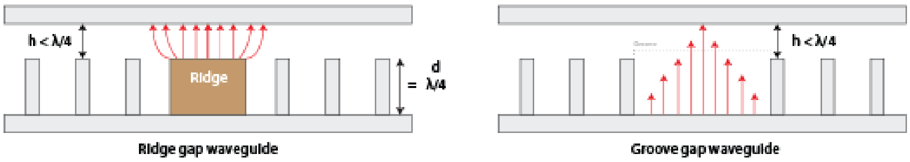

Figure 2.5: Comparison of frequency band designations

the pins (distance between the two metallic pins), the height of the air gap between the upper plate and top edge of the pins (pin gap). The stop band is set by the pin structures whereas the cutt off frequency of the guided waves is determined by the ridge or groove section. The pins period must be less than $\lambda/2$ at the center frequency, the pin gap defines the higher cutoff frequency of the stop band and should be less than a $\lambda/4$ at center frequency. The lower end cutoff frequency is determined by the width and height of the pins.
There are many advantages of the gap waveguide technology over the pcb technology and conventional waveguide which has been mentioned below:

- No metal contact is required between the two metal plates which reduces the losses as compared to the conventional waveguide where good metallic contact is necessary and could introduce losses due to non-ideal manufacturing process.
- Low-loss waveguide components can be manufactured at mmWave or even higher frequency bands allowing the technology to become a low-cost solution for various applicatons.
- When using conventional waveguides, multilayer structures could introduce field leakage due to necessary electrical contacts between them. However, these could be avoided in Gap waveguide technology due to no metal contacts.
- Gap waveguides are planar and cheaper to manufacture specifically at mmWave and higher frequencies.

2.5.2 Parallel-Plate stop band structures

Parallel plate stop band could be realised using various metallic structures. Some of them are given below:

1. Parallel-Plate cutoff realised by Bed of Nails
2. Parallel-Plate cutoff realised by Mushroom-Type EBG
3. Parallel-Plate cutoff realised by Bed of Springs
4. Parallel-Plate cutoff realised by zigzag wires/conical pins

We will discuss more about the cutoff realised by bed of nails. The basic principle remains the same for rest of the structures. A unit cell of circular pins could be taken into consideration for designing the stop-band which is shown in the figure 2.6. The pin shape (circular or square) is trivial to have any impact on the stopband.

The "gap height" (h) is an important parameter in deciding the parallel-plate stop band. The height is basically measured as the distance between the upper edge of the pin to the upper plate. To study the effect of the gap height we keep all the

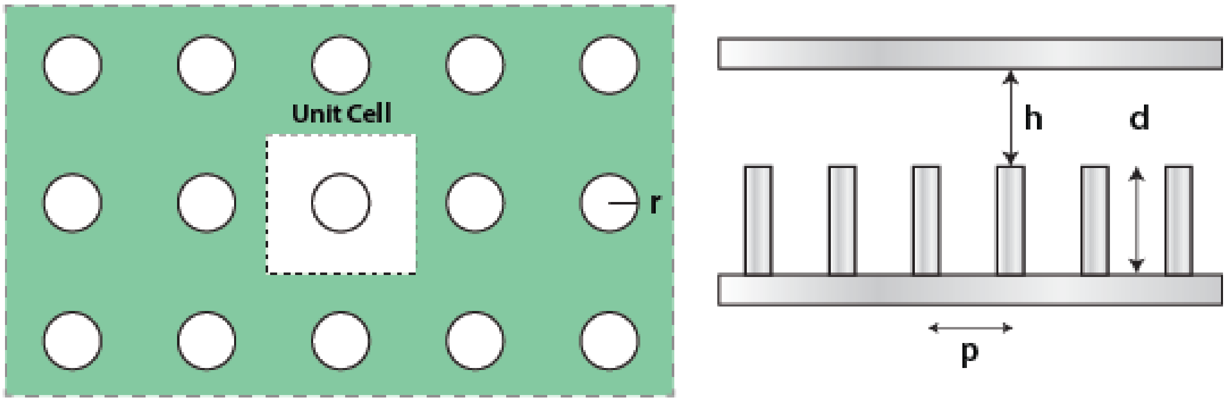

Figure 2.6: Top and side view of a unit cell arrangement

other parameters i.e periods of the pins (p) and length of the pin (d) constant. As the distance between the pins and upper plate decreases, the stop band increases. This becomes more prominent when the gap height varies with other parameters as well. In another case, when the period of the pins increases, the cutoff at the start frequency of the stop band reduces whereas the end frequency of the stop band is not changed if the period is small enough. The new modes could be propagated which reduces the upper end of the stop band drastically when the period becomes larger. However, the increase in the stop band is mostly because of the reduction of the start frequency when the period is larger than $\lambda/4$ because the upper cut-off frequency remains moreover same for small h. The radius-to-period ratio (r/p) affects the stopband as well. An important observation with respect to r/p is the movement of the stop band in opposite direction when it reaches a maximum ratio of 0.2 [15]. Based on the above theory, we can check the stopband for a unit cell and apply it to a bed of nails that could be incorporated with ridge and groove structures to manufacture a waveguide. We can optimize these parameters to decide the stopband frequency of operation and more details on a unit cell for D-band is explained in further section 3.3 of the report.

Applications for 30GHz and above are well suited for realising bed of nails structures. However, for low frequencies applications these structures often becomes bulky due to which it becomes more practical to look into other type of structures for achieving the requirements. The bed of springs shown in the figure 2.7 satisfy the requirement of being less bulky since the helix structure will provide the same depth that would be equivalent to the length of the helix structure. Another advantage of helix structure that it decreases the resonant frequency by generating equivalent inductance and capacitance of the cell structure. This concept can be applied to multiple frequency band but mainly for lower frequency applications. The distance between top plate and upper edge of the spring does not generate enough capacitive effect due to which the gap can be increased further to embedded other discrete components like capacitors, inductors, etc. for packaging unlike the case in bed of nails. The modes of the stop band can be reduced to lower frequencies by increasing the number of turns of the helix structure thus making the structure more compact [16].

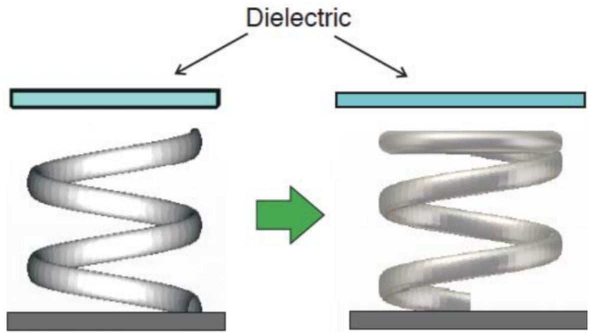

Figure 2.7: Unit cell of a helix structure [16]

Designing integrated antennas at millimeter frequencies have challenges in terms of the complexity of the MMIC circuits and resonance problem while packaging. One of the previous solutions used to have bond wires to connect the feed line with the input of the antenna. The efficiency of the antenna used to decrease because of the increased losses in the feeding network. A solution that included gap waveguide technology proved to be an efficient solution since the losses were reduced as there were no dielectric material involved to manufacture the waveguide along with isolated microwave circuits for integration with gap waveguide which will reduce the need of additional packaging solutions. The square pins with $\lambda/4$ height satisfying the PMC conditions are usually preferred for high frequency applications. However, in this case, due to the bond wires sticking to different parts of the circuit, the pin lid cannot be placed close to the bottom layer which restricts the gap and affects the parallel stop-band as shown in the figure 2.8a. Another type of geometry has been designed to solve this issue at 60GHz which is inverted pyramid-shaped nails 2.8b. The advantage of this structure that the length of the pin and distance between the top and bottom plate is similar to the square pin structure but there is a increase in the stop band from 62-92 GHz to 59-120 GHz which met the desired requirement with a low loss gap waveguide technology [17].

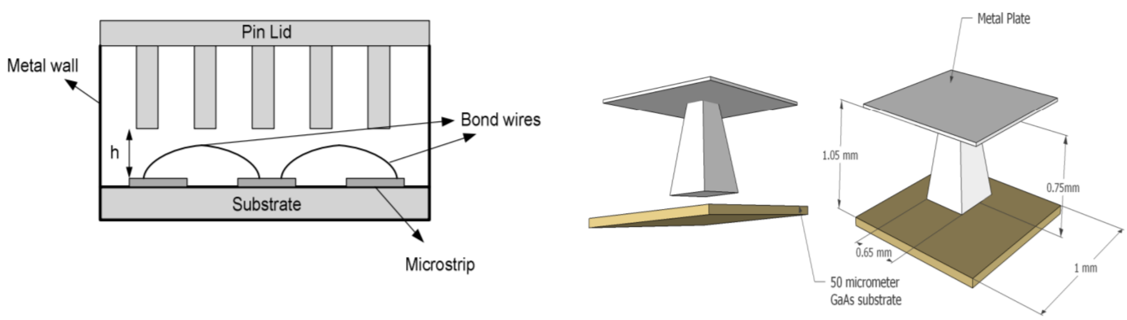

(a) Bond wire configuration for array antennas

(b) Unit cell for a inverted pyramid pin

Figure 2.8: Gap waveguide technology for Inverted pyramid pin structures [17]

2.6 Gap Waveguide Components

This section provides a brief introduction to different components that can be manufactured using gap waveguide technology. The transmitter, receiver and diplexer including antennas forms a complete unit for a full-duplex system and these components are manufactured using various technologies such as microstrip and coplanar that provides good integration compatibility and are easy to manufacture. However, at higher frequencies they suffer from losses and cavity resonances that can be overcome using gap waveguide technology. A short hybrid coupler at 38GHz providing coupling of 3dB along with isolation and return loss of 20dB has been implemented using groove gap waveguide. Similarly, a narrow-band band-pass diplex filter using groove gap waveguide resonators at 38GHz is implemented with a insertion loss of 1.5dB and return loss of 17dB. Antennas with high gain and directivity has been developed using gap waveguide technology that provides an isolation higher than 80dB for TX-RX to avoid crosstalk and feedback loops leading to system instability. The complete active microwave circuit of 38GHz radio link was packed using gap waveguide technology allowing a one-stop solution for a complete full duplex system [18].

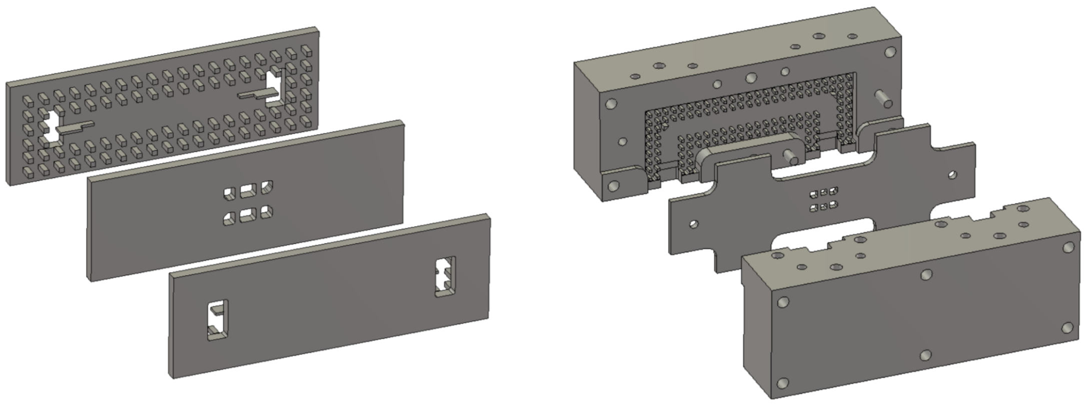

(a) Transition 1

(b) Transition 2

Figure 2.9: Coupler with different transition configurations [19]

A directional coupler is a passive device usually used as mixing signals, measurements of reflected signals, powere level and signal sources isolation for mmWave applications. A 60 GHz directional coupler using groove gap waveguide structure has been discussed further which provides advantages over the conventional coupler at mmWave frequency applications. In this design, two groove gap waveguide are placed parallelely one over the other sharing a common broad wall and are coupled to each other through apertures. A two row of holes is implemented in the broad wall for achieving the desired coupling. A three sets of double-hole aperture in the broad wall provides a coupling of 30dB and hence various sets of three, five, nine and eleven sets of double-holes were designed to achieve different coupling values of 30db, 25dB, 20dB, 15dB and 10dB. A compromise should be made to achieve the best results from good coupling, flatness and broadband performance. However, the coupling value can be only modified by changing the number of apertures. Two transition has been designed to couple the signal from gap waveguide to standard WR-15 rectangular waveguide out of which one includes ridge section with a step and extension to the waveguide opening to provide return loss of -15dB shown in the figure 2.9a and another includes four 90° bends along with two section step at the bottom wall of the groove waveguide to provide -24dB of return loss as shown in the figure 2.9b. The designs were fabricated and measured that provided reasonable results and some discrepancy due to the assembling tolerances and inaccuracies in fabrications [19].

Microwave filters are a vital part of multiple wireless system and it is realised using hollow rectangular waveguide in two separate metallic parts that are connected through screws. These conventional rectangular waveguide can sometimes be tedious to integrate with other active components on printed circuit board and hence an example of a V-band filter using gap waveguide technology that overcomes the former disadvantages has been mentioned further. A filter based on iris has been presented where the iris are formed by selecting the two pins with different sizes with respect to the square periodic pins used for creating the artifical magnetic conductor (AMC). Two transitions from groove gap waveguide to WR-15 is implemented using an aperture of a specific width at the pin plate. The width of the aperture and its position with respect to the back wall of the groove gap waveguide is used for improving the matching. For a fifth order chebyshev filter, the input and output coupling can be realised by the width of the first and last resonators which are closer to the apertures. Similarly, the inter-cavity coupling between the resonators can be determined by the insets between the iris as shown in the figure 2.10. The center frequency of the groove gap waveguide cavity can be controlled by changing the size of one of the width's of the input resonator. The design was fabricated and a minimum insertion loss of 1.7dB along with return loss better than 9dB with a fractional bandwidth of 1.34% at 59.7GHz was achieved [20].

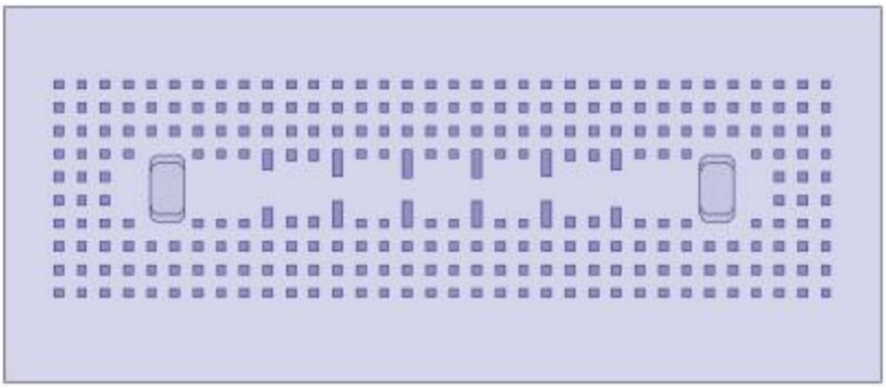

Figure 2.10: Proposed design for v-band filter using groove gap waveguide technology [20]

Gap waveguide technology has been used to develop array antennas for multiple frequency bands due to their low-loss performance, cost effectiveness and manu-

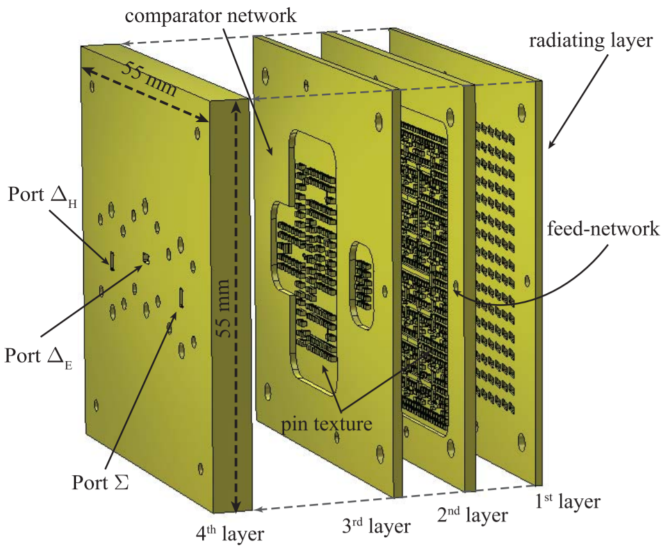

Figure 2.11: Monopulse array antenna [23]

facturing flexibility. A W-band monopulse slot array antenna with a wide band profile has been implemented using this novel technology. There are no galvanic contacts required among the different building blocks of the waveguide structure and it provides high efficiency along with wide impedance bandwidth (85-105 GHz). As shown in the figure 2.11, the 4 layers of waveguide structures does not require electrical contact and hence they can be screwed on the corners to obtain the array antenna and comparator network. The layer 1 is designed as the subarray for the array antenna which consists of three unconnected layers namely radiating layer, cavity layer and feeding layer. The radiating slots are excited uniformly with equal amplitude and phase and to achieve the desired uniformity and a wideband feed network, the design procedure described in [21] and [22] has been used to design the feed network. To achieve 32 dBi gain, Layer 1 has 16 x 16 array of radiating slots where a subarray is formed from each 2 x 2 slots and fed by a cavity on the top side of layer 2. A ridge waveguide feed network is used on the back of layer 2 to uniformly excite the feeding cavities of 8 x 8 array. Three Magic-Tees are embedded for the layer 3 to provide a coupling aperture of the sum signal and two difference signals in the E and H planes. The position of the three input ports at the layer 4 is used to excite the sum and difference patterns. The results for the proposed antennas are quite significant where insertion loss of the sum E and H plane difference is around 0.5 dB and return losses for the sum and difference ports are better then 10 dB. The antenna is well suited for millimeter wave tracking applications and more information is described in the article [23].

It is challenging for the available active circuits above 100 GHz to provide high data rates above 50 Gbps over a large distance for next generation backhauling systems using a single point-to-point link. There is a need for low-cost fabrication methods for waveguides above 100 GHz and hence a new technique has been mentioned in this section which utilizes low-cost polymer injection molding based fabrication

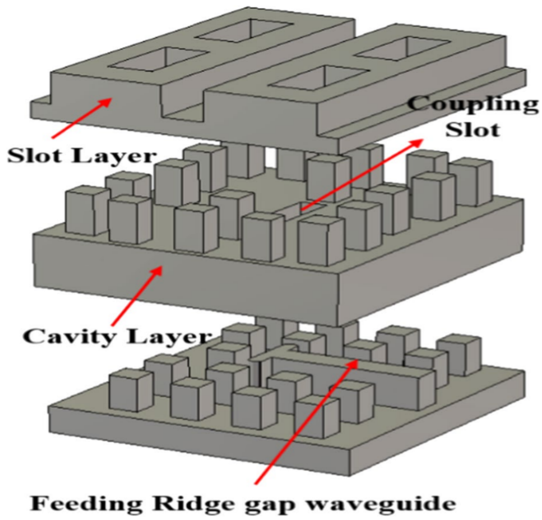

(a) Multi layer array

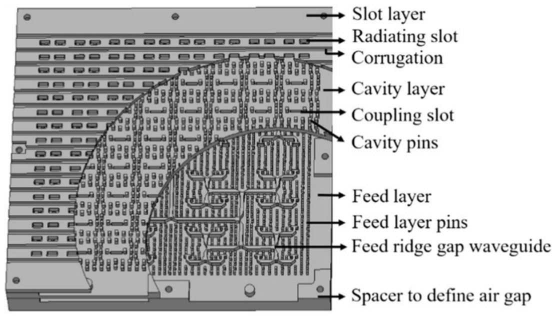

(b) 16X16 array antenna

Figure 2.12: Antenna design for 140 GHz slot array antenna [25]

solution for high gain antennas at 140 GHz. The gap waveguide technology has proved the one stop solution due to its non-contact nature of the waveguide. The slot arrays based on gap waveguide is preferred to design this antenna that operate at a bandwidth of more than 30%. Usually the wideband slot arrays require feed network and hence an intermediate cavity is used between the feeding layer and radiating slot layer as shown in the figure 2.12a. The working principle of this antenna is mentioned in [24] in detail. However, to achieve the broad side radiation, the antenna has been re-optimized for 140 GHz that enables the slots in each subarray to be excited with the same phase and amplitude. Sixty-three 3-dB power dividers has been cascaded that is embedded in the feeding layer and the electromagnetic energy is coupled to the cavity layer which is placed above the feeding layer. The figure 2.12b shows the multi-layer 16x16 element slot array antenna that is excited with a standard D-band waveguide flange. Here we need a transition from a normal rectangular waveguide to ridge gap waveguide which has been mentioned in the symmetric transition in [24]. To reduce the complexity of the fabrication process, micro-machining with a polymer was used to implement slot array gap waveguide antenna at 140 GHz. Master imprints for PDMS molds were made using SU8 and SU8 master for each layer was used to make PDMS molds. Milled AI injection molding were used along with PDMS molds which were later injected with OSTEMER. The S_{11} for the complete array is below -14dB for the band of interest(135-150 GHZ) along with 14% of bandwidth and 31 dBi gain at 140GHz. The performance of this array antenna can be improved more with reduced cost if could be done with the automated fabrication process and more details is presented in [25].

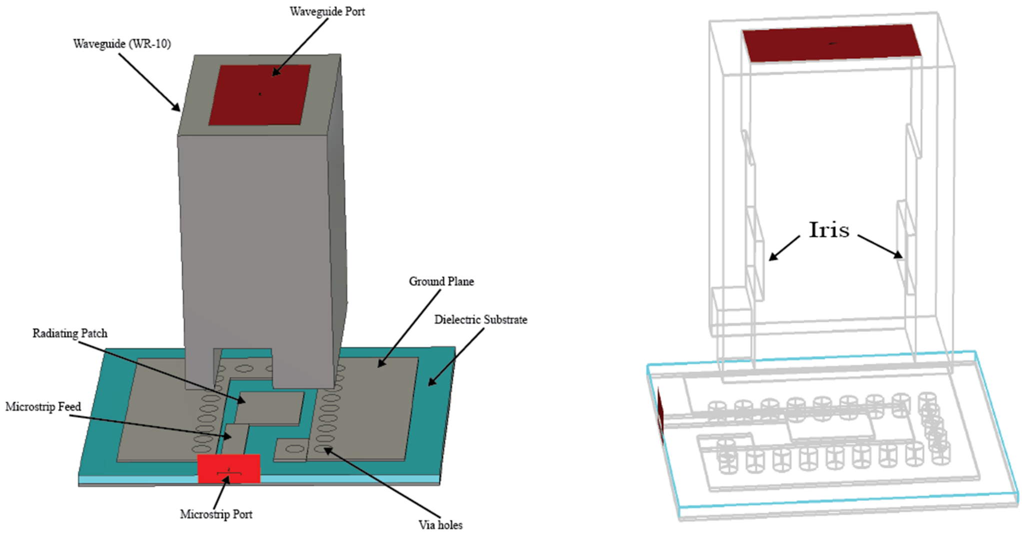

(c) Overview **(d)** Waveguide with Iris

Figure 2.13: H-plane Transition

2.6.1 Microstrip-Ridge Waveguide Transition

This section explains the working of a typical transition at a mmWave range. A working H-plane transition mentioned in the paper [26] has been referred for understanding the basic working and designing of a transition. There are many transitions that has been designed over the years and the basic concept is to have a good matching between the microstrip and a waveguide section to couple the signal for the desired frequency range. The design mentioned here has been divided in two different parts where one section focus more on the transition design and the other section focus more on adding features to the waveguide to increase the bandwidth of the overall transition. The figure 2.13 depicts an overview of the design that includes important components whereas, the other figure shows the waveguide with Iris that has been used to increase the bandwidth of the transition. A signal is fed through the microstrip port onto the feeding line that is connected to the radiating patch. The microstrip line exhibits quasi-TEM mode and the waveguide has TE_{10} as the dominant mode. To match the fields from a microstrip line to a waveguide, a patch antenna in the TM_{01} mode is implemented. To achieve wider bandwidth, Iris distance and height is varied that also increases the complexity of the structure. However, since the feed line is through the H-plane wall of the waveguide, It makes the design more compact to embed with other systems. The bandwidth achieved with this design is around 11% that can be increased to 15% by including Iris in the waveguide. More detailed information about the transition can be found in the following reference [26].

A gap waveguide technology is emerging as one of the advantageous solution for mmWave frequency bands. A transition is designed using this novel technology where desired electromagnetic waves are propagated between two PEC-PMC parallel-plate waveguide configuration. An artificial magnetic conductor (AMC) is emulated by a series of periodic structure in the form of metal pins. The top plate and the AMC together forms a stop band which then can be incorporated with a guiding structure in the AMC layer such as groove, ridge, strips to propagate the waves without being leaked from the periodic structure. The top plate and AMC does not have a physical contact which makes this technology more reliable as it suppress all surface waves or parallel-plate modes. In this design, the most essential requirement for a good transition is to transform the E-fields from the microstrip to the guiding structure.The domainant mode is Q-TEM mode in both microstrip and Ridge gap waveguide that makes it less complicated to transform the fields. This is achieved by extending and tapering down the width of the guiding structure (ridge in this case) to the same width as that of the microstrip (50Ω). The tapered sections needs to be in contact with the microstrip and this could be achieved in multiple ways (soldering, gluing) but in this design, the tapered ridge is pressed against the microstrip line that gives an advantage of replacing the faulty sections. A back-to-back structure was implemented to validate the concept of the proposed transition and a bandwidth of 10 GHz(23-43 GHz) was achieved with a S_{11} of -14.15 dB and S_{21} of 0.32 dB [27].

3
Method

This chapter provides the utilization methods of the finalized transition starting with a discussion about the software used to design the transition. Section **??** explains the structural details for the Gap Waveguide technology followed by the dielectric material in section 3.2. A H-plane transition was designed initially for 140 GHz which was later replaced by the E-plane transition. The design of these transitions along with their advantages and drawbacks is discussed in the section 3.4 and 3.5. The E-plane design proved to be more reliable and hence a section dedicated to check the robustness and efficiency have been mentioned in the section 3.5.3. The design has been manufactured and measured using B2B configuration due to the complexity of the structure and requirement of advanced tools to measure the design at mm-Wave frequencies. Multiple variants with different offset of the microstrip patch were manufactured considering the manufacturing error margin which will affect the results of the design severely is presented in the couple of last sections.

3.1 Simulation Tool

The final results from the measured transition were based on the designs and simulations done on a electromagnetic field simulation software called 'Microwave CST Studio suite' widely used for Electromagnetic (EM) simulations for various applications. The CST provide different solvers (time domain, frequency domain, eigenmode) which could be used depending on the requirements of the applications to achieve the best results.
In this work, Eigen mode and transient solver is used which utilizes the finite integration technique (FTT) to solve the design using hexahedral meshes. The software is flexible to generate accurate result by creating fine meshes but at the cost of increased CPU-time. There are several algorithm techniques that can be used for the design structures and one of them is genetic algorithm that has been applied for the design of the transition. The software provides the output data in various formats and you have the flexibility to either use MATLAB or Python to process these results further to a more readable format. Parametric studies can be performed to study various data points and effects of tolerances that might occur during the manufacturing process. This also provides us with certain data sets that can be used to define the robustness and stability of the transition over a certain range. CST also provides various export and import options. The export options allows various 2D 3D options which can be used with other CAD software to manufacture the designs.

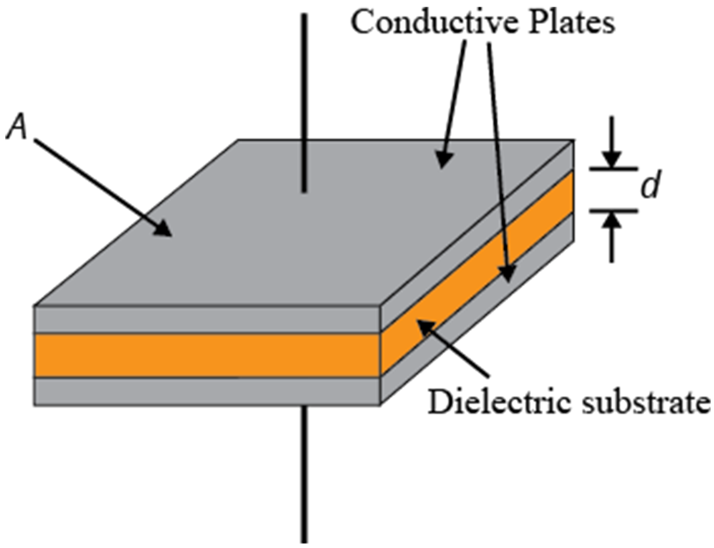

Figure 3.1: Dieletric Substrate

It is also compatible with other simulation softwares like HFSS, ADS [31].

3.2 Dielectric Materials

Dielectric materials are usually poor conductors that provides an insulating layer between the two conducting layers as seen in the figure 3.1. For the transition a pcb substrate with a dielectric material having specific properties suitable for this design. There are various dielectric materials available in the market and one with minimum dielectric loss is preferred for better performance. However, these less lossy substrates are usually costly specifically for the high frequency around 140GHz. Hence we have used a substrate which is optimized for 77GHz but less suited for frequency band of interest. The dielectric loss increases with the frequency and hence it is important to select the material which exhibits similar properties in practical application as mentioned in the data sheet [29]. Low dielectric constant (Dk) allows rapid signal propagation and low dissipation factor (Df) maximize the power delivered are the important parameters needs to be considered while selecting the dielectric materials. These values are usually mentioned on the data sheet provided by the manufacturer.

For the design in this report, Astra MT77 of copper thickness at 0.18mm has been used as a dielectric material which provides Dk = 3 and Df = 0.03 at 100 GHz. The substrate thickness is 0.127 mm with an additional FR-4 layer to provide sturdiness to the pcb otherwise it could be easily broken while assembling it with the waveguide using screws. The dielectric material is also comparable to other substrates such as Rogers 3003, however testing and implementation on radar technology has been performed with Astra MT77 at 77 GHz, which seems to be a promising technology for higher frequencies above 100 GHz. In addition to the above advantages, Astra

MT77 does not includes plasma process which makes the process cheaper reducing the substrate cost. The manufacturers provided the changes in dielectric constant and loss tangent for MT77 until 100 GHz in the specification sheet, however, a prediction has been done for both Dk and Df at 140GHz. [30].

3.3 Unit Cell

Section 2.5.2 provides a detailed explanation about designing a unit cell. The shape of the pins does not play a vital role in determining the stop band. The length of the pin(d), distance between the upper plate Pin(h), radius(R), and period(P) determines the stop band for a given frequency band. The effect of these parameters individually or combined have different results that has been explained in the section 2.5.2. To achieve a good stop-band for D-band(110-170) frequency, a circular pin structure has been used. The advantages of using a circular pin structure over a rectangular pin is merely simplicity during the manufacturing process. The manufacturing becomes complicated at such high frequencies since the size of the components becomes smaller. While milling the components, there are more curved edges rather than sharp edges (rectangular, triangle) and hence circular pins makes it easier to fabricate the pins. The figure 3.2a shows the top view and 3.2b shows the side view of the circular pins which were later used in the transition design.

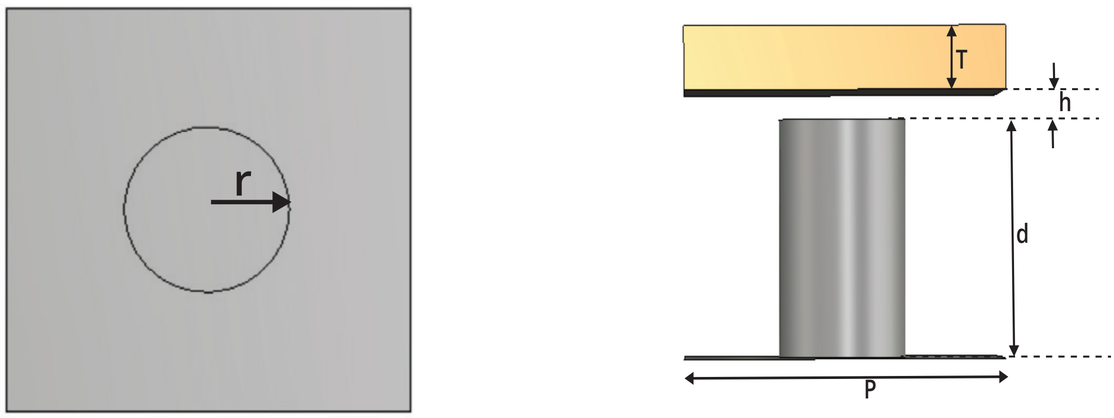

(a) Top View

(b) Side View

Figure 3.2: A unit cell for 110-170 GHz

The dimensions of the unit cell for 110-170 GHz has been done by following the principles and rules mentioned in the section 2.5.2. The table 3.1 shows the dimensions optimised to obtain a stop band of 98GHz (82-180 GHz). All these parameters have different effects on the stop band and a designer can optimise these range of a stop band depending on the applications. An observation can be made from the stop band range that the lower frequency has more margin (28 GHz) compared to the higher frequency (10 GHz). However, there are also some limitations as we move higher in frequency due to which it becomes difficult to achieve greater margin as

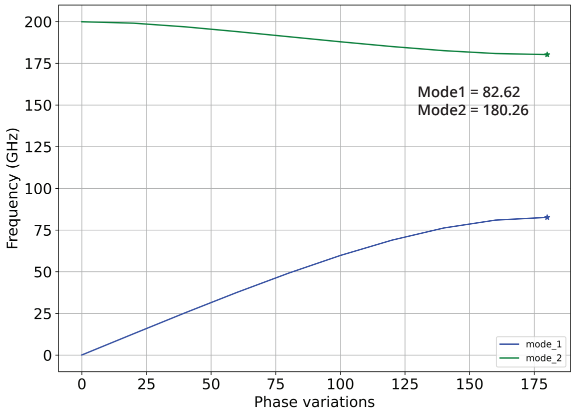

Figure 3.3: A unit cell for 110-170 GHz

compared to lower frequency.

Contents	Units(mm)
length (d)	0.48
period (p)	0.8
gap (h)	0.135
Thickness (T)	0.127
radius (r)	0.32

Table 3.1: Dimensions of a Unit cell for 110-140 GHz

The figure 3.3 provides a graphical view of the stop band where we have two mode1 & mode2 that defines the cut-off at lower and higher frequency respectively. The Eigen mode solver is used to calculate the fields of a periodic unit cell by applying boundary conditions in y-z direction. All the fields within the range of approx. 82-180 GHz will be propagated whereas frequencies outside this range will be blocked. As the structures does not behave ideally in a real world, we need to have some margin around D-band since there will be some resonances that might occur at the edges of the desired frequency. As mentioned earlier, these dimensions has been optimized to fit the criteria of obtaining a decent stop band with some margin along with satisfying the physical requirements of the pin for manufacturing purposes.

3.4 H-Plane transition

The motivation to design H-Plane transition for D-band is adapted from the former transitions mentioned in the section 2.6. The design in this section is scaled and adapted to work for the frequency band 110-170 GHz. The major difference in this design is that there is no physical contact between the H-plane waveguide and the ground plane. The reason for adaption is utilization of the Gap Waveguide technology where the rectangular waveguide WR-7 is embedded with the cylindrical pins as shown in the figure 3.4a. The dielectric substrate used here is MT77 which is 0.127mm thick with Tanδ as 0.003 at 100 GHz.

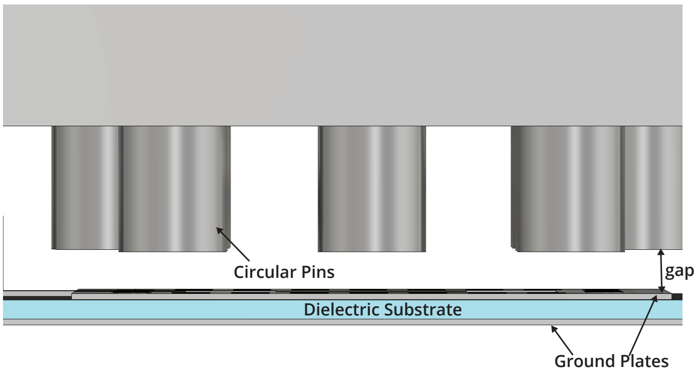

(a) Side View

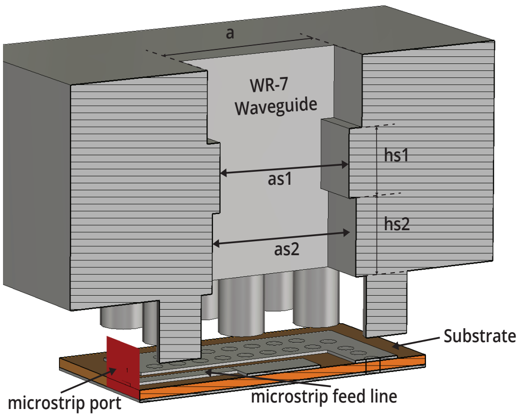

(b) Cross Section

Figure 3.4: H-Plane Transition waveguide

3.4.1 Waveguide

The waveguide has three different section of length as depicted in the figure 3.4. The as1 and as2 are varied depending on the requirement to achieve maximum bandwidth by maintaining a good insertion loss. The length and the position of the Iris inside the waveguide affects the bandwidth and hence the Iris length was optimized with different positions to obtain good results. The opening lengths of the waveguide (a) and (b) is the WR-7 waveguide lengths where the fields are measured or embedded with other applications. The fields from the microstrip patch is coupled to the waveguide through the opening with a length of as2. The waveguide is surrounded by the cylindrical pins that has a height of PinH and radius of PinR. These pins are designed for a stop band of 110-170 GHz and the further measurements specifications of the Pins can be found in the table 3.2. Ideally there should be infinite pins in X & Y direction to obstruct the leakage of fields. However, In practice, couple of rows are enough to prevent the field leakage. In this design, two rows of pins worked efficiently to couple the field from the microstrip patch to the

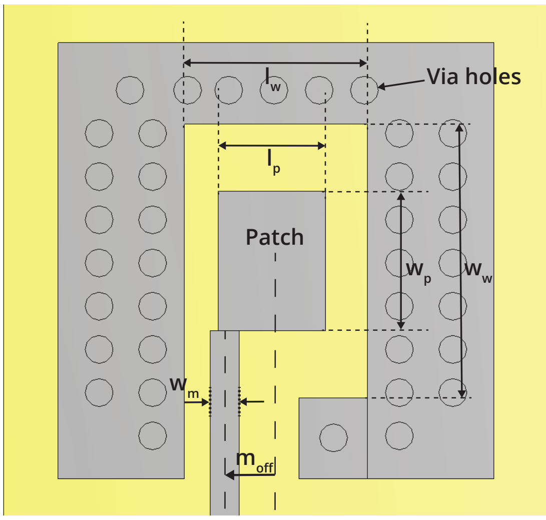

Figure 3.5: Top view of the patch

waveguide opening without any field leakage.

3.4.2 Microstrip Patch

The patch is designed on the MT77 substrate with a copper thickness of 0.02mm that are usually available in the market for the manufacturing process. The signal is fed through the microstrip line of 50Ω that is connected to the radiating patch. The dimension of the radiating patch is given in the figure 3.5 where the length is given by W_p and the width is given by I_p. The patch is centered with respect to the waveguide opening. The distance between the patch and the ground plane is same as the size of the waveguide opening i.e. I_w and W_w is same as the size of waveguide opening near the patch (b & as_2). The patch size is optimized to have a good matching with the waveguide for best coupling of the signal. The via holes are grounded through the substrate around the patch to suppress the parallel modes that might arise in the dielectric substrate. The placement and distance between the vias are not critical in terms of improving the overall performance.

3.4.3 Matching section

The microstrip line is directly connected to the radiating patch with a width of W_m and an offset of m_{off} from the center of the patch. The overall impedance matching and bandwidth is dependent on the location of the feed line along with the slot between the ground plane and the radiating patch [32]. The bandwidth shifts in terms of frequency bands with respect to the position of the feed line. The Patch and feed line are designed in such a way that they can move in the slot in any direction to achieve the best results. The patch along with the feed line is moved in various direction to check the tolerance of the structure. To increase the bandwidth, Iris dimensions and location has been changed to optimize the results which has been further discussed in the result section. The table 3.2 summarises the dimensions of the complete design.

Contents	Units(mm)
Height of Pin (PinH)	0.44
Period of the Pin (P)	0.38
Distance between the patch and Pins (gap)	0.15
Radius of the Pins (r)	0.38
Waveguide (a)	1.25
Waveguide (b)	0.89
Distance between iris (as1)	1.2
Distance between walls (as2)	1.33
Height of the iris (hs1)	0.49
Height of the wall (hs2)	1.15
Patch width (I_p)	0.52
Ground plane (I_w)	0.89
Patch lenght (W_p)	0.68
Ground plane (W_w)	1.33
Width of the feed line (W_m)	0.14
Offset from the center of the patch ($m_o ff$)	0.2

Table 3.2: Different measurement for H-plane design

3.4.4 Drawbacks

The design did not meet the expected requirement of bandwidth and hence the results were not satisfactory. Due to mmWave design, the units of the structure were very small and hence there would have been a difficulty in manufacturing a small offset of the feed line to the radiating patch. Since the fabrication does not have sharp edges and the design was sensitive to small changes, the results would have affected severely even with small margin of errors. This can be verified through the simulations results mentioned in the section results. The design was compact and would have been beneficial for integration to save space but if the requirement demands for wider bandwidth then we need another robust design which is presented in the section 3.5.

3.5 E-Plane

Due to the limitations with H-plane design, an E-plane transition was studied and implemented with two different matching section techniques. The motivation for the transition design was taken from one of the paper published on an E-plane transition for 77GHz [28]. The design presented in the paper is based on the vertical transition from microstrip to double ridge waveguide. The gap waveguide technology is implemented to prevent wave propagation in an undesired direction when surrounded around the patch and the waveguide port. The figure 3.6 shows two design of E-plane transition where 3.6a has $\lambda/4$ transformer as a matching section and 3.6b was implemented using the stub matching. The design was simulated and optimised in CST which is explained in detail in the section 4. The E-plane transition doesn't require via holes which reduced the manufacturing complexity and cost at the same time. The expectation from this design was to have a good matching and large bandwidth compared to it predecessors at 77GHz. The expectation for the bandwidth is about 25% of the total frequency band i.e approximately 15GHz of bandwidth with a low loss of around -0.3dB. The design is also expected to be robust for 100um of displacement in all the directions that accounts for uncertainties during manufacturing and integrating with other products.

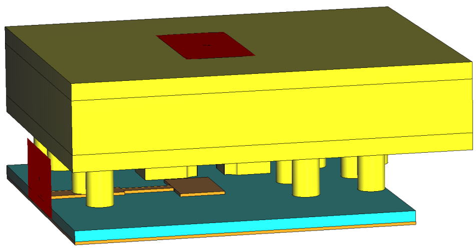

(a) Design with $\lambda/4$ Transformer

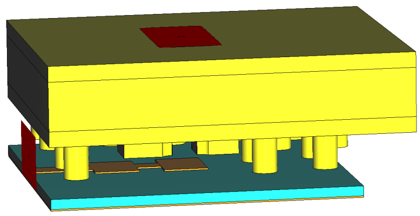

(b) Design with stub matching

Figure 3.6: E-plane design for D-band. Note: Some of the pins were removed from the design to show the components clearly.

3.5.1 Waveguide

The waveguide is manufactured from aluminium which also includes the ridge pins and circular pins. The figure A.2 shows various parameters of the waveguide which include three stages of waveguide section for transferring the signal from doube ridge waveguide to a WR7 rectangular waveguide. The section 1 is the ridge waveguide WR7 with the dimensions as 1.651mm X 0.8255mm. WRRH is the thickness of the ridge waveguide which does not affect the signal much and hence it can be modified according to the requirements. WRRA is the distance between the ridges which is the most crucial and sensitive part of the design that determines the cutt off frequency of the double ridge waveguide. The ridges in the section 1 and section 2 is optimized together to obtain the optimum results. The section 2 is the intermediate stage that transfers the signal from a ridge waveguide to a rectangular waveguide. The height of this section determines the transition of the fields to rectangular waveguide and hence INTH along with INTA plays an important role in the working of the waveguide. INTA is the distance between the ridges at the intermediate section. Finally, section 3 is the standard WR7 rectangular waveguide with the dimensions WR7B and WR7A. The thickness of this section does not affect the fields and hence it can be extended further depending on the applications. The edges of the ridge pins and waveguide slots were blended to have a curvature structure to ease the manufacturing process.

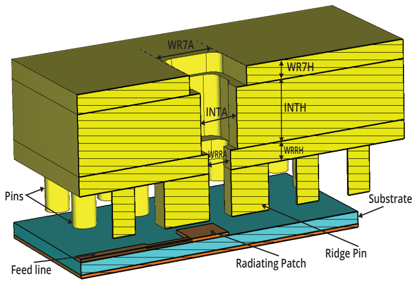

(a) Side View 1

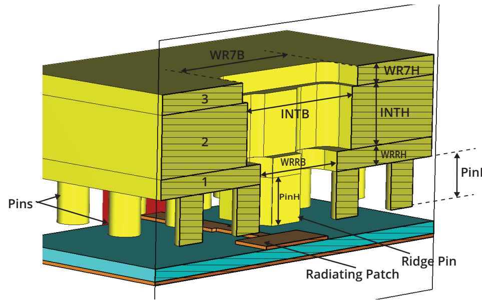

(b) Side View 2

Figure 3.7: E-plane side view

The figure 3.8 shows the bottom and top view of the waveguide where the patch is aligned at the center in one of the lateral direction whereas it has some offset in other lateral direction that is considered the nominal case for this design. The INTRH is the width of the ridge at the intermediate section which is a bit wider compared to the width of the ridge pins and ridge present at the ridge waveguide section(WRRH). From the figure 3.8a, the blended edges is quite visible at the corners for the all three sections of the waveguide. The same profile has been maintained during the manufacturing process which has been presented in the section 3.7. The ridge pins are extended towards the PCB on each side to couple the fields from the patch to the waveguide as shown in the figure 3.8b. The width and length of the ridge pins are sensitive and affects the matching of the PCB to the waveguide. The width of both the ridge pins are same and given by RiW whereas the lengths are given as RiH1 & RiH2. The distance between the pins is given by period that applies in both X & Y direction. The pins are not well aligned through out the waveguide due to the different lengths of the rigde pins but it maintains the distance of period in all the directions. The distance between the top of the pins and the surface of the patch is 0.15mm which is the nominal case for the design.

The E-plane transition does not require via holes to suppress the cavity modes which makes the fabrication of the PCB's to be cheaper and less complex as compared to the former H-plane design. The bandwidth provided by E-plane is about twice the H-plane and hence it is viable to optimize the E-plane transition to achieve better results. The matching sections in E-plane transition is easier to fabricate as contrary to the H-plane where the margin of error was less.

3.5.2 Matching section

Two matching techniques were implemented to compare the performance and effects of different matching structures on the design. These two variants of the matching technique that has been implemented for this design: Stub & quarter wave transformer. The signal is fed through a 50Ω line having a width of Lin_W for both the matching techniques. The figure 3.9a has a width of W_PS f & height of H_PS for the radiating patch. The stub is connected through a small section of the microstrip line with a width of W_MS and a height of H_MS. The stub is designed

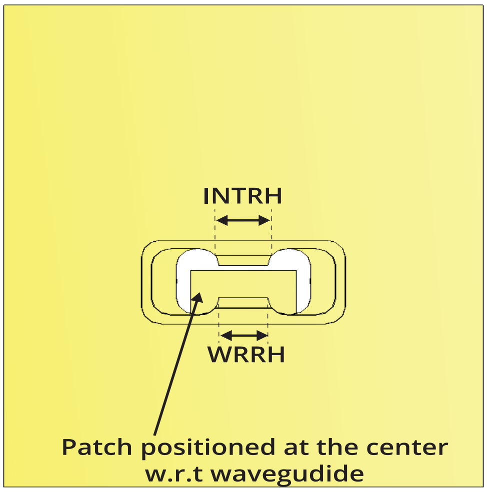

(a) Top View

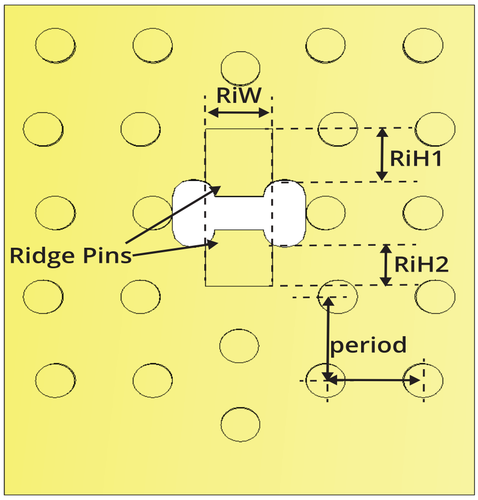

(b) Bottom View

Figure 3.8: E-plane Top & Bottom view

and optimized in parallel with the dimesions of the patch to provide good matching at the center frequency of the D-band. The width and height of the stub patch is given by W_SS & H_SS respectively. The figure 3.9b shows a $\lambda/4$ matching section where the width and height of the radiating patch is given as W_PQ & H_PQ and W_MSQ & H_MSQ for the width and height of the quarterwave section. The thickness of the microstrip patch and ground plane is 0.018mm and the material used is copper.

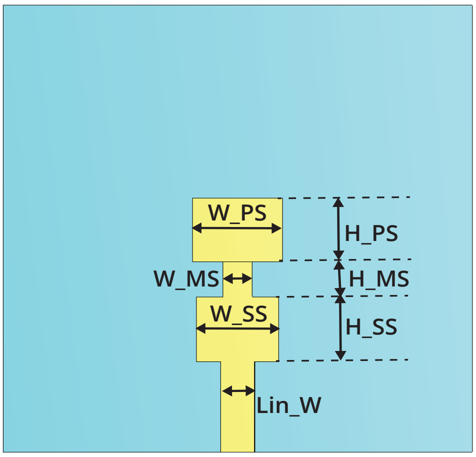

(a) Stub Matching

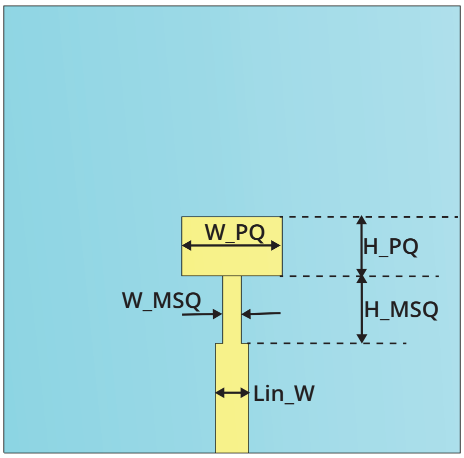

(b) quarterwave matching

Figure 3.9: Matching Techniques

3.5.3 Tolerance check

There will always be a deviation between simulation and manufactured prototypes in terms of their dimensions. In the design presented here, two different structures needs to fabricated and since we are working at D-band, the structure becomes smaller and increases the complexity to fabricate them with high precision. Hence, a tolerance analysis has been performed by changing the parameters of the structures. In case of the waveguide structure, effects of changes in the gap between the ridges along with the dimension of the ridge pins were studied which are the most crucial part that could severely affect the performance of the design. Similarly, in terms of the matching section, several variants of different sizes were fabricated assuming the error margin of 10% provided for the fabrication of the PCB's provided by the manufacturer. The microstrip section was displaced with respect to the waveguide in one of the lateral direction to determine how tolerant the design is to the misalignment between pcb and the waveguide. The detailed discussion and analysis has been presented in the section 4.

3.6 B2B structure

For simplicity, a B2B structure was implemented to test the working of these designs as shown in the figure 3.10. The other option to the B2B structure is to have the microstrip connectors instead, but due to very high frequency applications, it is impractical to perform the testing. The same structure presented in the figure A.2 was replicated along the x-axis and connected together by extending the waveguide walls along with the circular pins with a distance of period between the pin structures. The physical diameter of each flange is 19.05 mm and hence the total length must be greater than 39mm along with some margin. There are two transitions that takes place at the opposite ends from the microstrip patch to the waveguide and hence the total loss could be calculated as:

$$\text{Total loss} = 2 \text{ x transition loss} + \text{microstrip line loss} \tag{3.1}$$

To calculate the losses in the microstrip line, another design with extra 10 mm of microstrip line was designed and compared to the actual design length of 24.3 mm. However, in this case we need another waveguide structure with increased length of 10 mm so that we can align the waveguide ports to the patch. This would add extra cost for manufacturing a waveguide structure to test a single PCB. To solve this issue the waveguides were split in two different sets which did not affect the performance at all and reduced the manufacturing cost into half for testing multiple length of PCB.

3.6.1 Split Design

The split design is shown in the figure 3.11 where the two waveguides can be move apart and closer to each other depending on the length of the PCB's. The waveguide has 3 screw holes, 2 guiding pucks and 4 alignment pins on each of the waveguide. The guiding pucks are a piece of metal embedded on the PCB's for better alignment

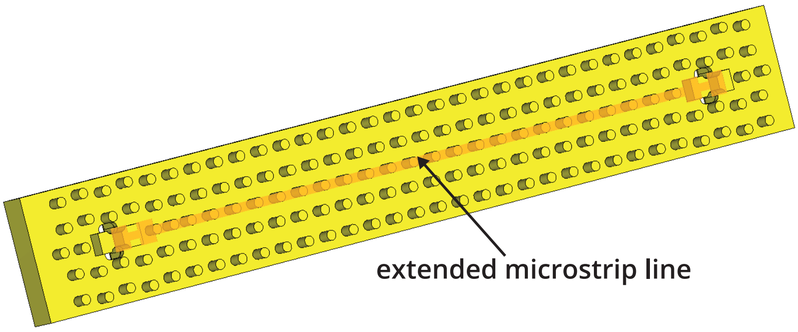

Figure 3.10: B2B structure

as shown in the figure 3.13. The alignment pins are used to align the waveguide flange towards the mechanical piece, whereas the surface mounted pucks are used for aligning the mechanical piece towards the PCB. In ideal case the split design is a replica of the figure 3.10 with more additional details that has been manufactured for final testing.

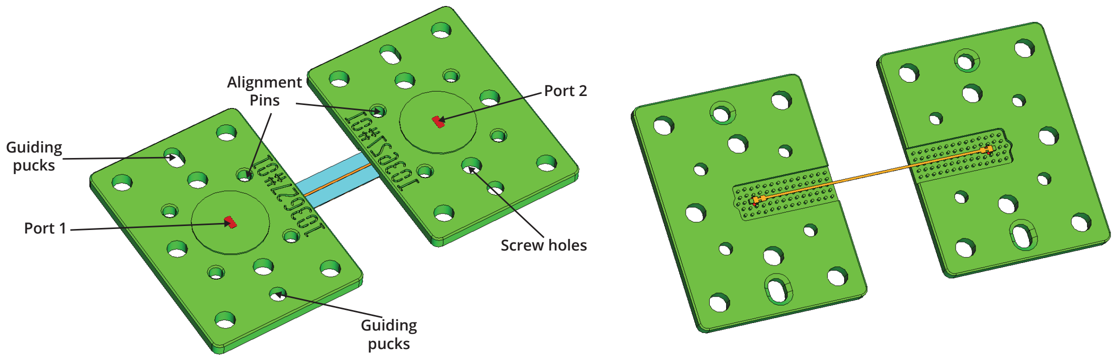

(a) Top View (b) Bottom View

Figure 3.11: B2B split design

The table 3.3 provides detailed information regarding the dimensions of the transition design.

3.7 Fabrication

The waveguides were fabricated using aluminium material and a milling bit of 0.3mm. The manufacturers provided a tolerance band of 10% but the final product was not precise as expected due to which there were some inconsistency in the waveguides as shown in the figure 3.12. The microscope view shows the misalignment and the dimensions seems to be not up to the tolerance. The share edges from the design for the ridge are not curved and also have some slope which will affect the performance. The distance between the waveguide ridges are a bit larger increases the gap between the ridge section for both ridge waveguide and intermediate

Contents	Units(mm)	Contents	Units(mm)
WR7A	0.65	Period of the Pins	0.8
WR7B	1.1	W_{PS}	0.77
WR7H	0.2	W_{MS}	0.25
INTA	0.52	W_{SS}	0.7
INTB	1.5	H_{PS}	0.57
INTH	0.63	H_{MS}	0.315
WRRA	0.32	H_{SS}	0.58
WRRB	1.1	W_{PQ}	0.88
WRRH	0.2	W_{MSQ}	0.16
PinH	0.48	H_{PQ}	0.53
INTRH	0.46	H_{MSQ}	6
WRRH	0.4	Lin_{W}	0.29
RiW	0.55	Thickness	0.135
RiH1	0.5	B2B length (length of the microstrip)	22.3
RiH2	0.4	Exended length	10

Table 3.3: Dimensions for E-plane transition design

section. This will affect the bandwidth of the design and introduce more mismatch losses. It is challenging to achieve high precision at such high frequencies when the structures becomes smaller and hence one of the major requirement of the design was to be robust. It is usually expensive to do the milling for such high frequencies for increased precision.

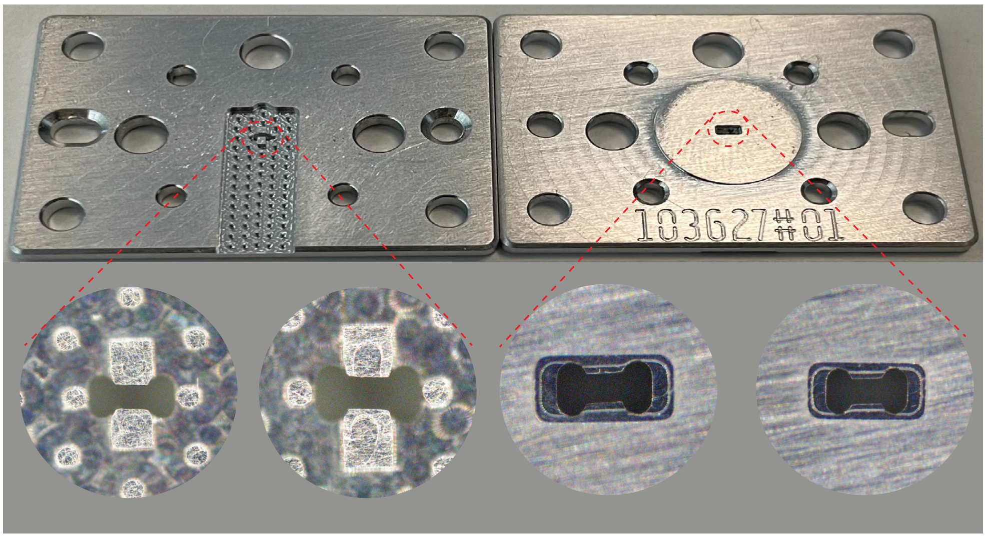

Figure 3.12: Fabricated Waveguides and microscopic view

The PCB's were manufactured with MT77 as the substrate and an extra layer of FR-4 substrate is added at the bottom of the PCB to provide extra strength. The substrate thickness is 0.127mm which could be easily broken due to fragile nature of the PCB. Two versions were manufactured, with and without silver coating on top of the copper in order to determine the impact on loss. No nickel were used while manufacturing the PCB that could generate some losses due to impurities. The figure 3.13 shows the copper and silver plated stub and quaterwave matching PCBs. Total 21 different PCBs were manufactured which included the nominal design along with different tolerance analysis and extended version of ideal case for the loss calculation. These variants were manufactured for both copper and silver and hence total 42 PCBs were produced. Since the design were compact, there was a possibility to replicate the same number of PCBs and hence finally total 88 PCBs were produced. The pucks are implemented on the PCBs to provide better alignment in addition to the guiding pins and screw holes.

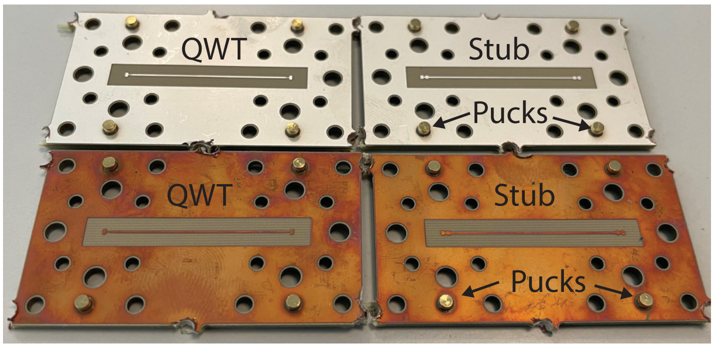

Figure 3.13: Copper and Silver PCBs

3.8 Measurement Setup

The measurement was done in one of the high frequency measurement labs at Chalmers University of Technology. The microscope were used at Chalmers and Gapwaves to analyze the deformations in the waveguides shown in the figure 3.12. Measurements were also done for the dimensions of the waveguide to figure out the distance between the ridges along with its height and length that would be useful to replicate the structure in the CST simulations. The details of the components required for the measurements of the transition is given in the table 3.4.

Contents	Quantity
Network Analyzer	1
VNA extender	2
90° waveguide bends	2
Cables per extender	4
Screws	8

Table 3.4: Components required for measurements

The figure 3.14 shows the complete setup where a Network analyser is connected to WR6.5 VNA extenders. The network analyser has a limited capacity to measure the S-parameters upto 26.5GHz and hence VNA extenders for D-band were used to extend and measure the S-parameters for the range 110-170GHz. The signals are fed to frequency extenders from the VNA and multipled it to desired frequency band is provided to the DUT through a D-band waveguide and received at the other frequency extender where the signal is filtered and down converted to the network analyzer. The calibration kit(D-band) was used to calibrate the flanges and VNA extenders to the desired reference point. The 90° waveguide bends are connected to the metal pieces and the distance is adjusted based on nominal or long line PCB case. The PCB is then placed on both of these flanges and pressed properly to fit in alignment with the guiding pins and pucks. Screws are tighten from top for both the waveguides to make sure that there are no gaps between the PCB and waveguides walls.

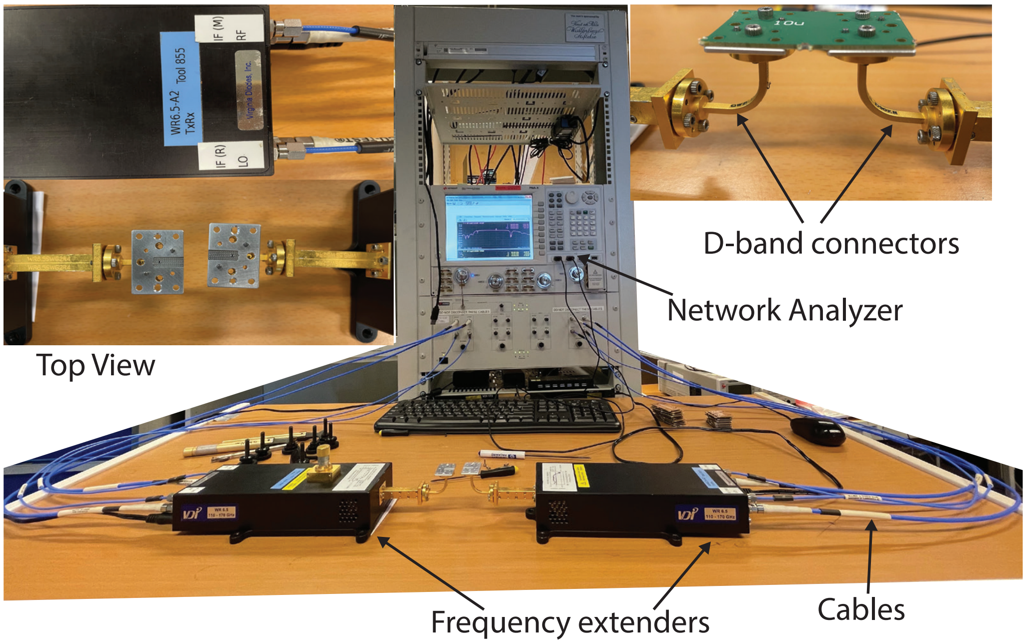

Figure 3.14: Measurement Setup

4

Results & Discussions

This chapter provides in depth details regarding the simulation results of the designs that were presented in the previous section. The results are presented for both measurements and simulations done in CST. The calculation for the losses in a microstrip line has been presented in further sections.

4.1 H-plane

The results presented here is based on the simulation results and no prototype were manufactured for H-plane design. As per the details provided in the section 3.4, H-plane was not able to provide sufficient bandwidth. The figure 4.1 shows the bandwidth of about 18 GHz which is calculated for S11 < -10dB. The matching is good at the center frequency of about 140-145 GHz which was expected as the transition was designed for the center frequency of 140GHz. The parameters such as $as1$, $as2$, $hs1$, $hs2$, Wp, Ip, m_{off} were varied which did not further improve the results. The tolerance performance was good when the waveguide was displaced by $\pm 100um$ in all directions. The results for the tolerance analysis has been mentioned in the Section A.

4.2 E-plane

4.2.1 Single ended transition

The single ended transition as shown in the figure 3.6a and 3.6b are the nominal cases that would be implemented in an actual application and the figure 4.2 shows the behaviour of these transitions in terms of bandwidth, insertion loss and return loss.

The figure 4.2a shows the simulated results on CST for quarterwave matching with a wideband response of 37 GHz that is almost twice of the H-plane design for the frequency range between 121GHz to 158GHz. The insertion loss is less than -0.4dB between 125-155GHz along with a bandwidth of 26% for the total D-band frequency. The resonances are been generated at 160 GHz that could be due to the substrate thickness. Although, the circular pins are designed for the stop band between 110-170GHz, it could be due to the pin stopband combining with the former condition for these undesired resonances. The waveguide has been displaced in lateral direction by $\pm 100um$ and $\pm 0.075um$ in vertical direction to check the robustness of the design.

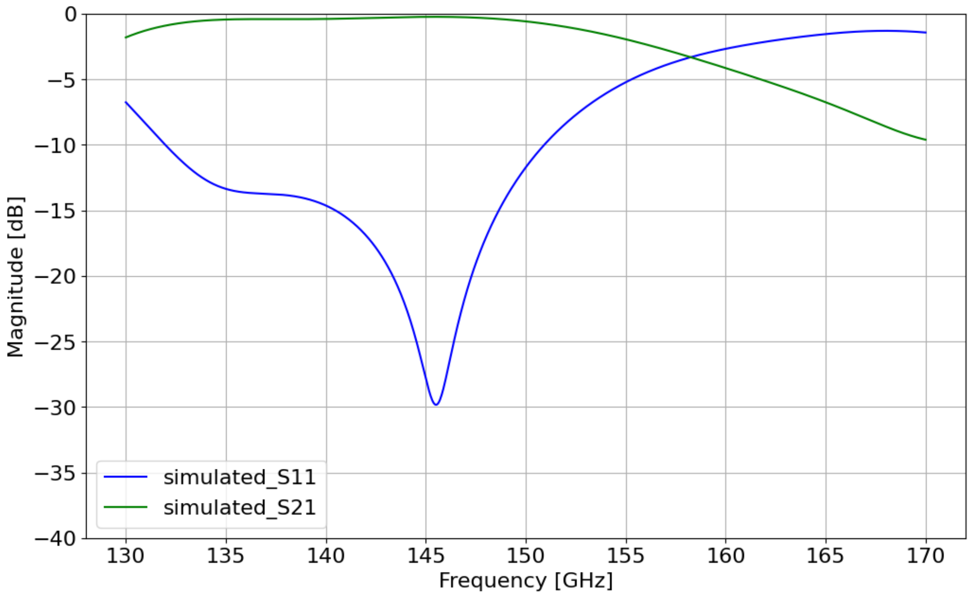

Figure 4.1: H-plane result

Out of total 27 variants there are only two cases which is shown in the section A where transition matching degrades at 145GHz, otherwise the design maintains its stability throughout the range of 125-155GHz. The results for tolerance analysis has been shown in the section A. The figure 4.2b shows the results for single ended transition with stub matching with a wideband response of 43GHz that is better than the quarterwave matching. The transition works in the frequency range of 120-163 GHz with a insertion loss less than 0.4dB for the range of 124GHz to 159GHz. The bandwidth achieved is around 30.71% which is 18% better than the former matching technique. The tolerance analysis for stub matching is similar to that of the quarterwave where for couple of cases, the matching seems to be degraded. However, these conditions were in most extreme cases where the waveguide is completely out of alignment with the radiating patch. The resonances are observed at 163 GHz which is better compared to the $\lambda/4$ matching. Detailed figures for tolerance analysis has been mentioned in the section A.

4.2.2 B2B design results

As mentioned in the section 3.6 B2B structures were manufactured and tested the performance of the transitions. The figure 4.3 shows the result for the ideal case of stub and quarterwave matching for B2B structures. The figure 4.3a shows the quaterwave matching results where the reflections between the ports are observed due to the back-to-back structure. The resonance follows the pattern shown in the figure 4.2a with a increase in insertion loss due to two transitions and extra losses from the increased length of the microstrip line. The insertion loss is still less than 3dB for the frequency range 124GHz to 152GHz with a overall wideband response of for S_{11} of -15dB level. The matching in the back-to-back structure could become

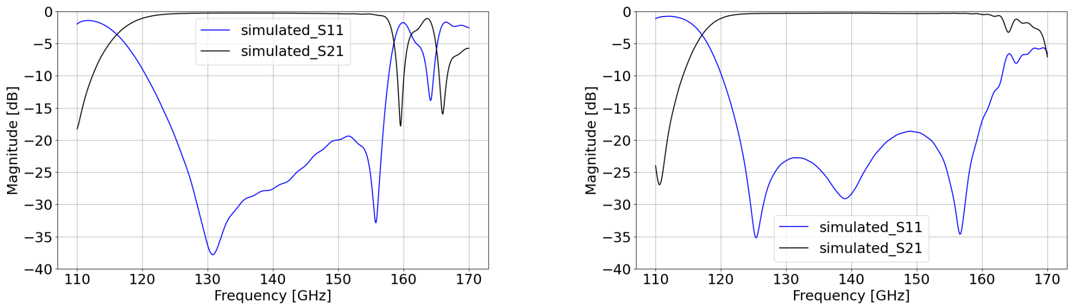

(a) $\lambda/4$ matching (b) Stub matching

Figure 4.2: Simulated result for E-plane

6dB worse as compared to the single ended transition due to the reflection between the ports in the structure. The figure 4.3b shows the results that follows the pattern for single ended stub transition. The insertion loss is less than 3dB for the frequency range between 122GHz-157GHz with a bandwidth of 40GHz. The resonances in both the back-to-back structures is approximately 6dB worse compared to the single-ended transition that makes the design more sensitive for higher frequencies. The tolerance analysis has not been performed for B2B structures since it is expected to have same behaviour as for the single ended transition. However, different variants of stub and quarterwave matching transition was manufactured which include under etching and over etching of the PCB's. The Patches along with the matching section was also displaced along the length of the waveguide to verify the robustness of the design. The figures has been mentioned in the section A along with the comparison of the measured results.

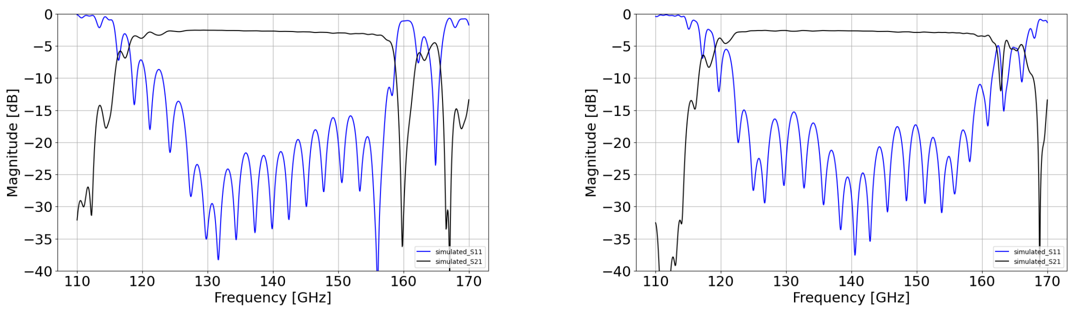

(a) $\lambda/4$ matching (b) Stub matching

Figure 4.3: B2B E-plane simulated results

4.2.3 Loss calculation

An extra length was added to the microstrip line to evaluate the loss in the microstrip line. The patches are manufactured with and without silver coating on top of the copper to improve the ohmic losses while working with different materials. The extended line variant was manufactured for the quarterwave matching since the type of matching will not affect the losses in the microstrip line. The figure 4.4 shows the measured results for the extended microstrip line for both with and without silver coating on top of the copper material. The figure 4.4a shows the simulated result for the extended microstrip line. The focus here is not to achieve a better bandwidth or insertion/return losses but to compare the two lines and achieve the losess per mm. The figure 4.4b shows the measured result from the fabricated silver and copper materials. A small bump is observed for the S21 of the copper material at 140GHz which due to imperfect calibration of the measurment setup. The calibration was done again later and the bump was not present for further measurements. However, the response for both silver and copper plating microstrip line is quite similar which shows that there is not a significant improvement in terms of losses even if the silver coated line is used. One of the reason for the loss could be the copper beneath the line has high surface roughness that is causing the majority of the loss and hence the contribution from the silver coating has hardly any effect on the overall loss of the system.

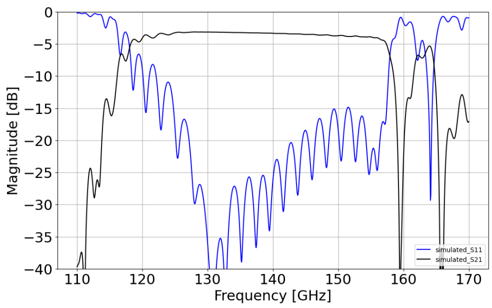

(a) Simulated extended line

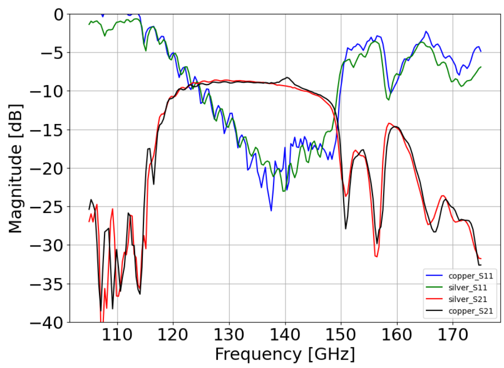

(b) Silver and copper coating

Figure 4.4: Simulated long line result and comparison of the measured lines for both silver and copper coating

The loss per mm is calculated by selecting fixed points and subtracting the losses from nominal line to the long line.

$$\text{Resultant loss} = \frac{\text{(Long line loss - nominal line loss)@fixed frequency points}}{\text{length of the long line - length of the nominal line}} \tag{4.1}$$

The figure 4.5 shows the comparison between the extended line and nominal line along with the losses in dB per mm. The extended line follows the nominal case pattern except the losses that is higher in the extended line. The difference is not huge but still silver seems to perform better than copper coating. The average losses for silver is 0.22dB/mm whereas for copper it is 0.25db/mm. The frequency range is chosen between 125GHz-147GHz because the matching works between these frequencies and for rest of the frequencies it becomes worse. The losses per mm can be multiplied with the total length of the microstrip line and divided by 2 i.e the losses in each transition section.

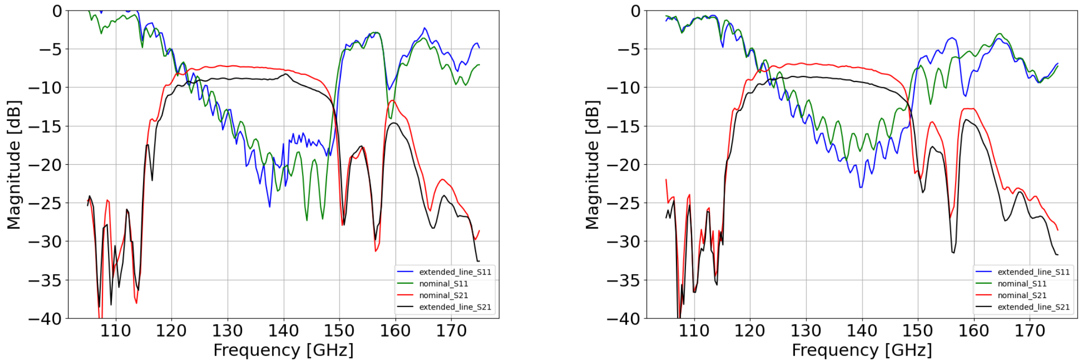

(a) Extended and nominal line - Copper **(b)** Extended and nominal line - Silver

Figure 4.5: Extended and nominal line for copper and silver

4.2.4 Measured results for B2B transition design

The measured results are presented in figure 4.6 for both silver and copper coating. However, the comparison is focused with more silver coating since the calibration was fixed during the measurements of silver coated PCB's which eliminates the bump at 140GHz and avoid confusions. However, the results are presented in the section A for further reference. The figure 4.6 shows the nominal case for both quarterwave and stub matching silver plated PCB's. The result for quarterwave matching shows that the bandwidth is 23GHz along with the insertion loss of 7.5dB around the center frequency of 140GHz. Hence the bandwidth comes down to 16.4% from the ideal 26.5% in the CST simulations. For the stub matching, the wideband response is 24.5GHz and the insertion loss is -7.6dB around the center frequency. The bandwidth is 17.5% compared to the 30.71% which was obtained from the simulations. The main reason for such huge deviations are the improper material characteristics, high frequency that makes the measurements sensitive to small changes, deformities in the waveguide structures specially at the ridges and intermediate section. The losses for the complete length(24.3mm) of the microstrip lines is around 5.33dB for 140 GHz. After subtracting this loss from the overall transition loss for the working band, we get an average loss of 2.14dB which finally provide the loss per transition of around 1.07dB at 140 GHz.

As mentioned earlier that many variants were fabricated to make sure that optimum results are achieved even if there are over etching and under etching problems. The following figure 4.7 shows various quarterwave and stub matching techniques which has better matching compared to the nominal case. The insertion loss and return loss of these variants are better than the nominal case. However, from the graph itself, it could be determined that the matching for some of the variants perform better which signify that the nominal case has some deformities and the other variants are closer to the nominal case. The other reason could be that the etching has been done perfectly but due to the deformities in the structures, one of the variants fits the conditions for perfect matching and hence we see better results for these variants. From the figure 4.7b & 4.7c it could be seen that the matching around the center frequency is better compared to the nominal case. The same pattern could be seen

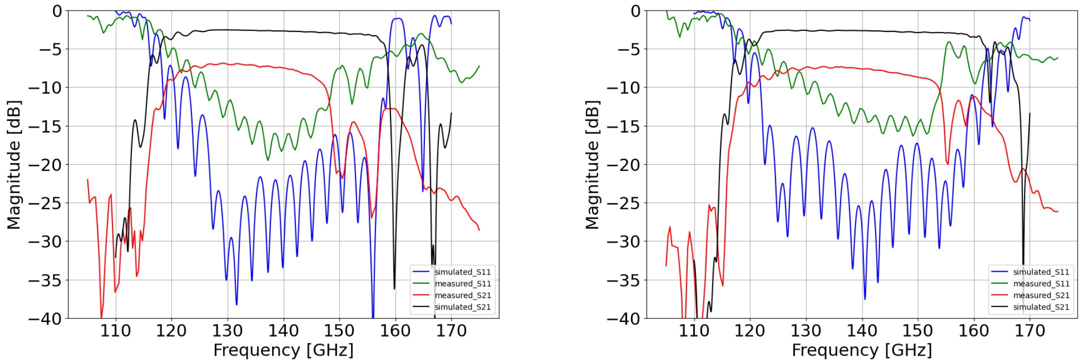

(a) Comparison of Quaterwave Matching (b) Comparison of Stub matching

Figure 4.6: Comparison of simulated and measured results for stub and quaterwave matching

for the stub matching as well in the figure 4.7d & 4.7e. The rest of the variants degrades in matching and insertion loss similar to the simulations in CST and have been presented in the section A for further references.
The insertion loss was quite high as compared to the simulations, and hence the $tan\delta$ of the substrate was changed to 0.09 that provided reasonable insertion loss during the simulation as shown in the figure 4.4. The loss tangent was significantly increased in the simulation results and the results were compared to the measured results. The loss tangent of 0.09 seems to match the simulated results which was then taken into consideration. This was done to simplify the simulation and account for all other impurities such as surface roughness on the copper/in the waveguide, impurities in the waveguide holes, misalignments etc. The insertion loss was increased to 0.6 dB for back-to-back configuration which is almost similar to an average of 7.5dB for the measured transitions.

The figure 4.9 shows the comparison between all the cases where the results with increased loss tangent have similar resonances to the simulated results. However, the losses have increased and closer to measured results. Hence, a conclusion can be made that the reduction in bandwidth is not because of the substrate losses but more due to the other factors like misalignment, impurities in the copper PCB and waveguide etc.

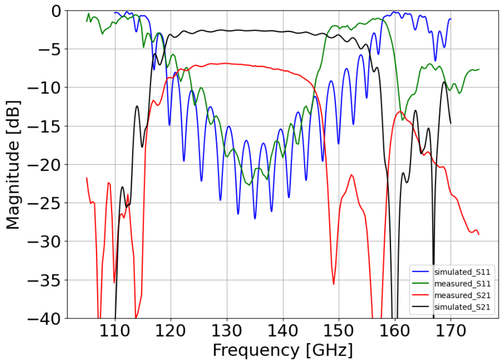

(a) Quaterwave - Displaced by -100um

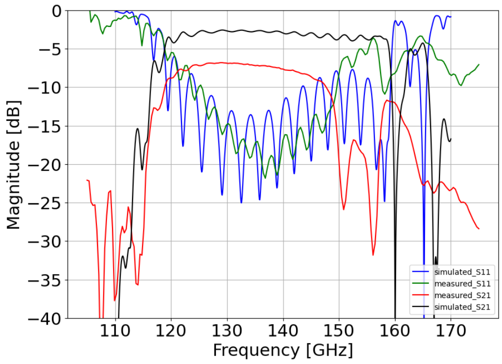

(b) Quaterwave - Over etching by 10um

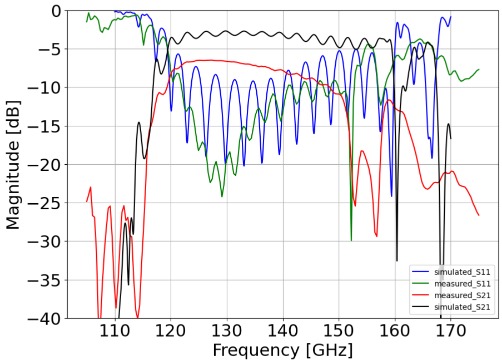

(c) Quaterwave - Over etching by 20um

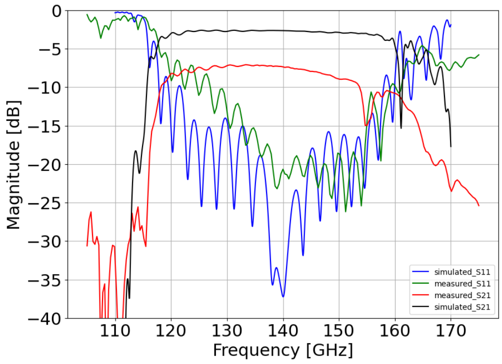

(d) Stub - Over etching by 10um

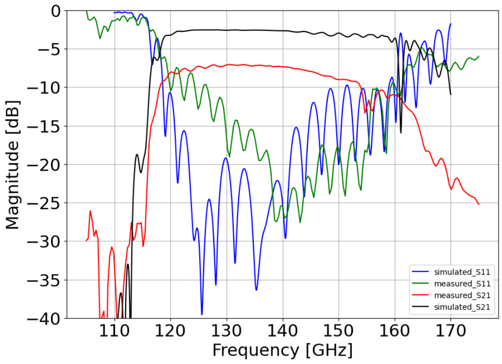

(e) Stub - Over etching by 20um

Figure 4.7: Different variants of the quaterwave and stub matching PCB's

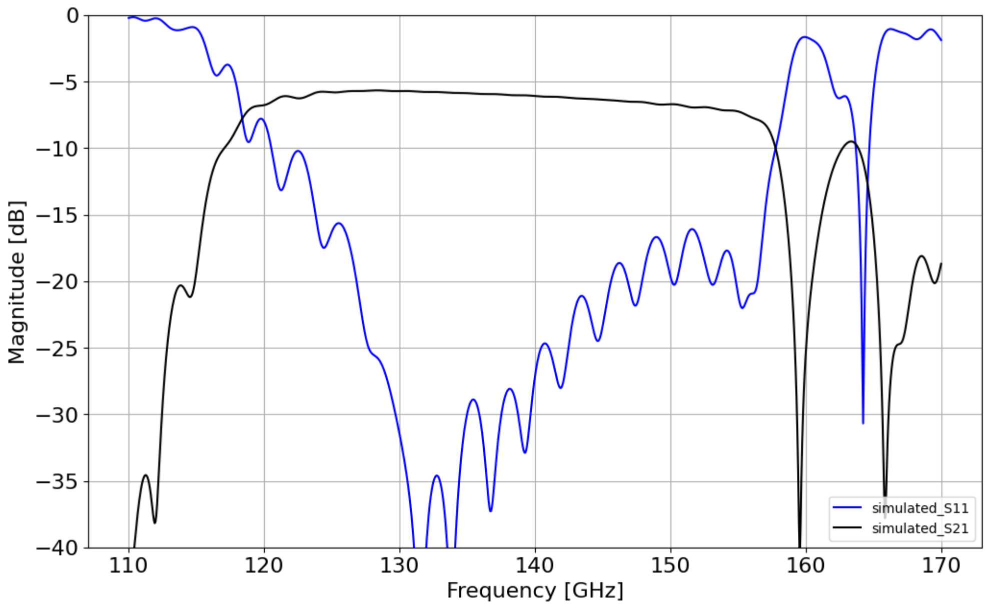

Figure 4.8: Loss Tangent changed to 0.09

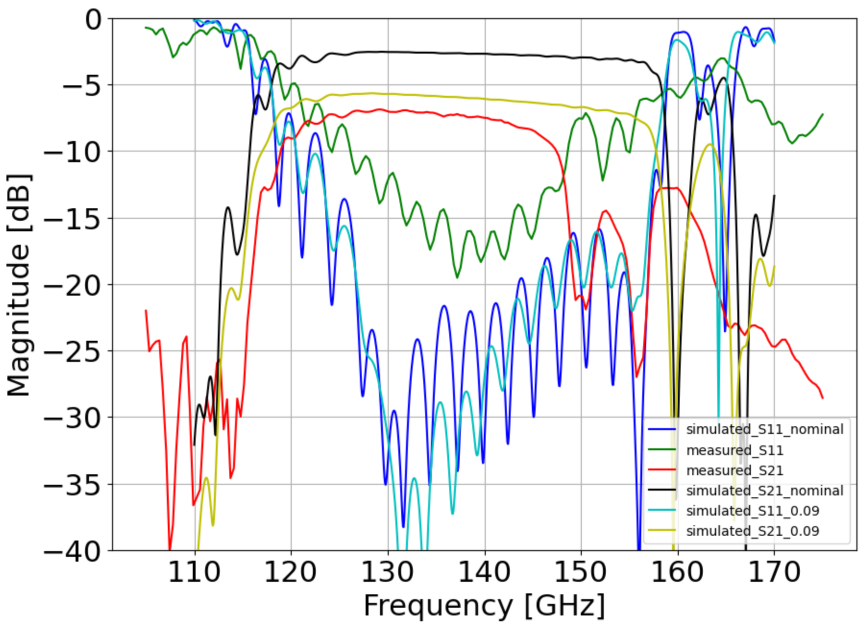

Figure 4.9: Comparison of measured, simulated and increased loss tangent results

5

Conclusion & Future Scope

The thesis work have explored the possibility of integrating microstrip line with gap waveguide for D-Band applications. Considering 140GHz as the center frequency, the quarterwave matching has 16.4% and stub matching achieved 17.5% of bandwidth after measuring the transition designs. The design performed as expected in terms of robustness and produced stable output throughout the testing of multiple variants. The stub matching seems to provide higher bandwidth compared to the quaterwave matching for simulated and measured results. The silver coating PCBs have better losses compared to the copper PCBs which makes silver coated PCBs a reliable option for manufacturing. The material characteristics plays an important role in terms of insertion loss since the behaviour of the material varies as the simulations moves up higher in frequency. The $\tan\delta$ had a difference of 0.06 while simulating and measuring the structures. The tolerances analysis provided ample amount of details to understand the behaviour of the structures specially in the higher frequency around 150-160 GHz. Some of the structures that were manufactured with some added tolerance performed better compared to the nominal case. Hence, a conclusion could be made that the manufactured design for nominal case were not the same as the simulated nominal case. The actual ideal case could be around somewhere between the nominal and displacement designs for the manufactured transitions. The tolerance analysis for under and over etching of the PCBs works until 20um and hence the fabrication needs to be done at high precision if higher performance stability is required. The design is quite compact and can be accommodate in small spaces for mmWave applications.

5.0.1 Future Scope

The material chosen was ideal for frequency up to 80GHz and hence different materials could be explored for D-band frequency that could provide better results. The manufacturing of the ridge section was not under the tolerance defined by the manufacturers and hence the waveguide structures can be manufactured with less deformities to provide better bandwidth specially at higher frequency points. The matching could be further improved by exploring other types of matching that can provide good insertion and return loss for the desired bandwidth. The waveguide structure itself can be improved by modifying the sensitive parts(ridge pins) to less complicated design structures that can provide room for better tolerance handling capacity of the transition design.

Bibliography

[1] J. Hasch, E. Topak, R. Schnabel, T. Zwick, R. Weigel and C. Waldschmidt, *Millimeter-Wave Technology for Automotive Radar Sensors in the 77 GHz Frequency Band* in IEEE Transactions on Microwave Theory and Techniques, vol. 60, no. 3, pp. 845-860, March 2012, doi: 10.1109/TMTT.2011.2178427.

[2] M. Fujishima, M. Motoyoshi, K. Katayama, K. Takano, N. Ono and R. Fujimoto, *98 mW 10 Gbps Wireless Transceiver Chipset With D-Band CMOS Circuits* in IEEE Journal of Solid-State Circuits, vol. 48, no. 10, pp. 2273-2284, Oct. 2013, doi: 10.1109/JSSC.2013.2261192.

[3] *https://docdb.cept.org/document/2012*

[4] Mesodiakaki, A., Kassler, A., Enrica, Z., Mattias, F., Tao, C. (2016) *Energy Efficient Line-of-Sight Millimeter Wave Small Cell Backhaul: 60, 70, 80 or 140 GHz* in World of Wireless, Mobile and Multimedia Networks (WoWMoM), 2016 IEEE 17th International Symposium on A IEEE URL: https://doi.org/10.1109/WoWMoM.2016.7523521

[5] David M. Pozar. *Microwave Engineering.* Wiley, 2012. ISBN: 9781118213636 URL: `http://search.ebscohost.com/login.aspx?direct=trueAuthType=ssodb=cat07472aAN=clec.EBC2064708site=eds-livescope=sitecustid=s3911979authtype=ssogroup=mainprofile=eds.`

[6] Horta, C. [Carol]. (n.d.). Chart of electromagnetic Spectrum [Pinterest post]. Retrieved June 22, 2021,

[7] A. Salcedo and E. Martinez, *Analysis of the Electromagnetic Spectrum under the Extremely Low Frequency Band: Frequency Sub-Bands Classification* 2017 International Conference on Mechatronics, Electronics and Automotive Engineering (ICMEAE), 2017, pp. 157-162, doi: 10.1109/ICMEAE.2017.15.

[8] Kildal, P. *Foundations of Antenna Engineering: A Unified Approach for Line-of-Sight and Multipath(Hardback) - 2015 Edition. Artech House Publishers*

[9] G. Casu, C. Moraru and A. Kovacs *Design and implementation of microstrip patch antenna array.* 2014 10th International Conference on Communications (COMM), 2014, pp. 1-4, doi: 10.1109/ICComm.2014.6866738.

[10] Per-Simon Kildal et al. *Design and experimental verification of ridge gap waveguides in bed of nails for parallel plate mode suppression.* Chalmers University of Technology, 2011.
URL: `http://search.ebscohost.com/login.aspx?direct=trueAuthType=ssodb=ir01368aAN=cpl.141224site=eds-livescope=sitecustid=s3911979authtype=ssogroup=mainprofile=eds.`

[11] Sharma, S., Tripathi, C. C., amp; Rishi, R. (2017). *Impedance matching techniques for microstrip patch antenna* Indian Journal of Science and Technology, 10(28), 1–16. *URL: https://doi.org/10.17485/ijst/2017/v10i28/97642*

[12] Kuester, E. F. *Theory of waveguides and transmission lines* CRC Press, an imprint of Taylor amp; Francis.

[13] Kildal PS, Zaman AU, Rajo-Iglesias E, Alfonso E, Valero-Nogueira A (2011) *Design and experimental verification of ridge gap waveguide in bed of nails for parallel-plate mode suppression* Microwaves Antennas Propag IET 5(3):262–270. doi:10.1049/iet-map.2010.0089

[14] Polemi A, Maci S, Kildal PS (2011) *Dispersion characteristics of a metamaterial-based parallel-plate ridge gap waveguide realized by bed of nails* Antennas Propag IEEE Trans 59(3):904–913. doi:10.1109/TAP.2010.2103006

[15] Rajo-Iglesias, E. ; Kildal, P. (2011) *Numerical studies of bandwidth of parallel-plate cut-off realised by a bed of nails, corrugations and mushroom-type electromagnetic bandgap for use in gap waveguides.* IET Microwaves, Antennas Propagation, vol. 5(3), pp. 282-289.
URL: `https://publications.lib.chalmers.se/records/fulltext/138299/local_138299.pdf`

[16] E. Rajo-Iglesias, P. Kildal, A. U. Zaman and A. Kishk *Bed of Springs for Packaging of Microstrip Circuits in the Microwave Frequency Range* IEEE Transactions on Components, Packaging and Manufacturing Technology, vol. 2, no. 10, pp. 1623-1628, Oct. 2012, doi: 10.1109/TCPMT.2012.2207957.

[17] A. Uz Zaman, V. Vassilev, P. Kildal and A. Kishk, *Increasing parallel plate stop-band in gap waveguides using inverted pyramid-shaped nails for slot array application above 60GHz* Proceedings of the 5th European Conference on Antennas and Propagation (EUCAP), 2011, pp. 2254-2257.

[18] E. Alfonso, A. U. Zaman, E. Pucci and P. Kildal *Gap waveguide components for millimetre-wave systems: Couplers, filters, antennas, MMIC packaging* 2012 International Symposium on Antennas and Propagation (ISAP), 2012, pp. 243-246.

[19] D. Zarifi, A. Farahbakhsh and A. U. Zaman *Design and Fabrication of Wideband Millimeter-Wave Directional Couplers With Different Coupling Factors Based on Gap Waveguide Technology* in IEEE Access, vol. 7, pp. 88822-88829, 2019, doi: 10.1109/ACCESS.2019.2926233.

[20] M. Rezaee, A. U. Zaman and P. Kildal *A groove gap waveguide iris filter for V-band application* 2015 23rd Iranian Conference on Electrical Engineering, 2015, pp. 462-465, doi: 10.1109/IranianCEE.2015.7146259.

[21] A. Vosoogh, P.-S. Kildal, and V. Vassilev, *Wideband and high-gain corporate-fed gap waveguide slot array antenna with ETSI class II radiation pattern in V-band* IEEE Trans. Antennas Propag., vol. 65, no. 4, pp. 1823–1831, Apr. 2017.

[22] A. Vosoogh, M. S. Sorkherizi, A. U. Zaman, J. Yang, and A. A. Kishk, *An integrated Ka-band diplexer-antenna array module based on gap waveguide technology with simple mechanical assembly and no electrical contact requirements* IEEE Trans. Microw. Theory Techn., vol. 66, no. 2, pp. 962–972, Feb. 2017

[23] A. Vosoogh, A. Haddadi, A. U. Zaman, J. Yang, H. Zirath and A. A. Kishk, *W-Band Low-Profile Monopulse Slot Array Antenna Based on Gap Waveguide Corporate-Feed Network* in IEEE Transactions on Antennas and Propagation, vol. 66, no. 12, pp. 6997-7009, Dec. 2018, doi: 10.1109/TAP.2018.2874427.

[24] D. Zarif, A. Farahbakhsh, A. U. Zaman, and P. Kildal *Design and Fabrication of a High-Gain 60-GHz Corrugated Slot Antenna Array With Ridge Gap Waveguide Distribution Layer* IEEE Transactions on Antennas and Propagation, vol. 64, no. 7, pp. 2905-2913, 2016.

[25] Farjana, S., Ghaderi, M., Zaman, A.U. et al. *Realizing a 140 GHz Gap Waveguide–Based Array Antenna by Low-Cost Injection Molding and Micromachining* J Infrared Milli Terahz Waves 42, 893–914 (2021). https://doi.org/10.1007/s10762-021-00812-8

[26] E. Topak, J. Hasch and T. Zwick *Compact Topside Millimeter-Wave Waveguide-to-Microstrip Transitions* IEEE Microwave and Wireless Components Letters, vol. 23, no. 12, pp. 641-643, Dec. 2013, doi: 10.1109/LMWC.2013.2284824.

[27] A. Uz Zaman, T. Vukusic, M. Alexanderson and P. Kildal *Design of a Simple Transition From Microstrip to Ridge Gap Waveguide Suited for MMIC and Antenna Integration* IEEE Antennas and Wireless Propagation Letters, vol. 12, pp. 1558-1561, 2013, doi: 10.1109/LAWP.2013.2293151.

[28] A. Bagheri, H. Karlsson, C. Bencivenni, A. Haddadi, T. Emanuelsson and A. A. Glazunov. *Microstrip to Ridge Gap Waveguide Transition for 28 GHz Steerable Slot Array Antennas* 2020 14th European Conference on Antennas and Propagation (EuCAP), 2020, pp. 1-4, doi: 10.23919/EuCAP48036.2020.9135076.

[29] F. Fereidoony, S. Chamaani, M. A. Sebt, and S. A. Mirtaheri *Efficient method for estimation of the thicknesses and complex dielectric constant of wall.* The 8th European Conference on Antennas and Propagation (EuCAP 2014), 2014, pp. 3085–3088
`URL: https://ieeexplore.ieee.org/document/6902480`

[30] Isola *PCB Material Selection for RF, Microwave and Millimeter-wave Design.* Microwavejournal.Com. (2014, May 8). [Slides].
`URL: https://www.microwavejournal.com/ext/resources/Webinars/2014/SLIDES_Isola_8may14.pdf`

[31] CST Microwave Studio `URL: https://www.cst.com/products/csts2/optimization/global-optimizer. Acquired 2021-09-30.`

[32] S. Pandey and R. Ramadoss *Coplanar patch antenna fed at the non radiating edge* Proc. IEEE Antennas Propag. Soc. Int. Symp., 2004,vol. 3, pp. 3397–3400.

A

Appendix 1: Additional results

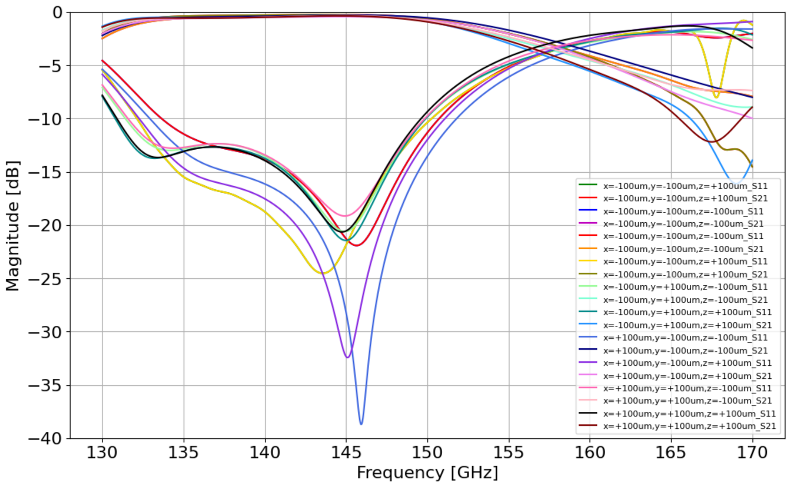

Figure A.1: Tolerance simulations for H-Plane transition

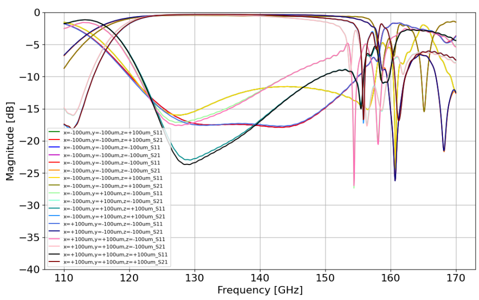

(a) Quaterwave matching

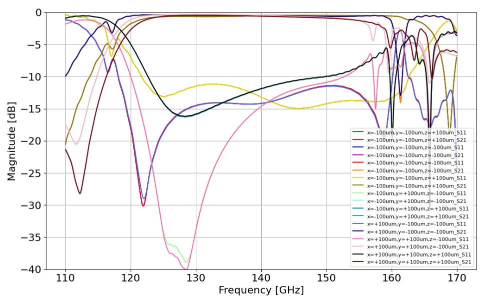

(b) Stub matching

Figure A.2: Tolerance analysis of single ended transition for $x = \pm 100um$, $y = \pm 100um$ & $z = \pm 75um$

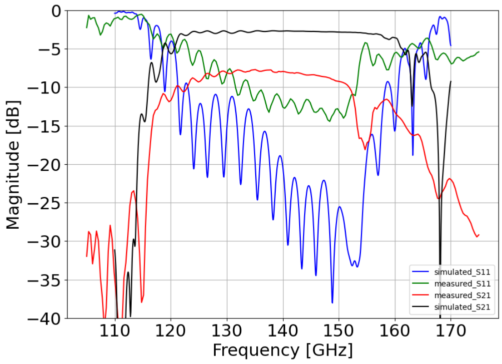

(a) Stub - Under etching by 10um

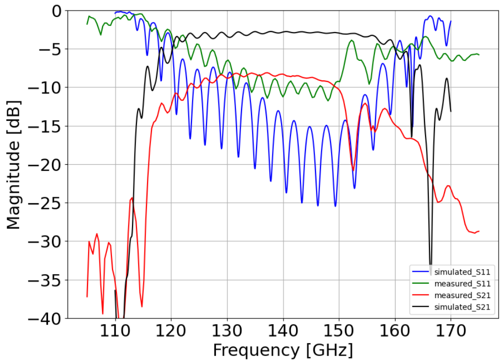

(b) Stub - under etching by 20um

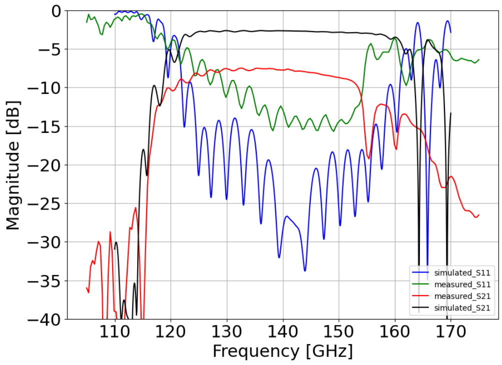

(c) Stub - Displaced by +50um

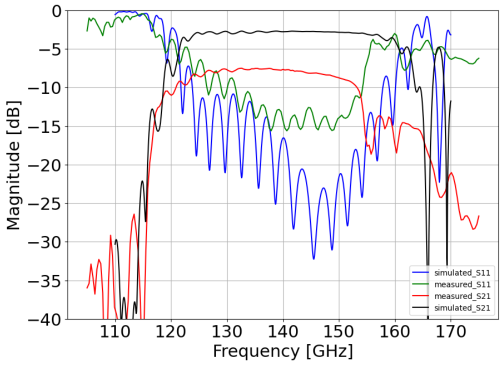

(d) Stub - Displaced by +100um

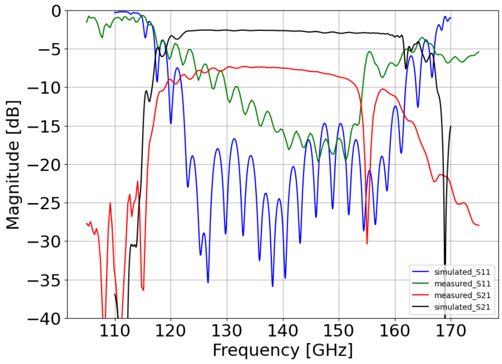

(e) Stub - Displaced by -50um

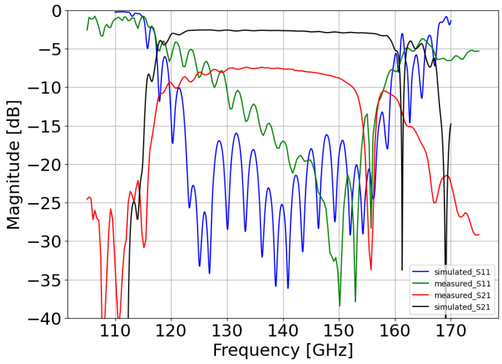

(f) Stub - Displaced by -100um

Figure A.3: Tolerance of simulated and measured results for Stub matching

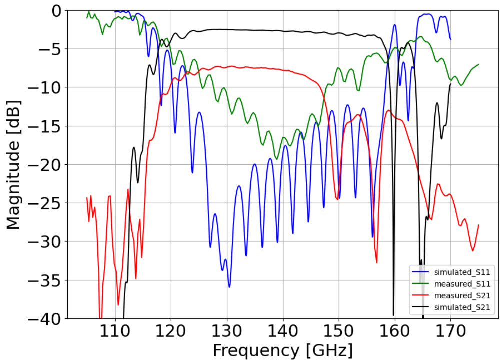

(a) $\lambda/4$ - Displaced by +50um

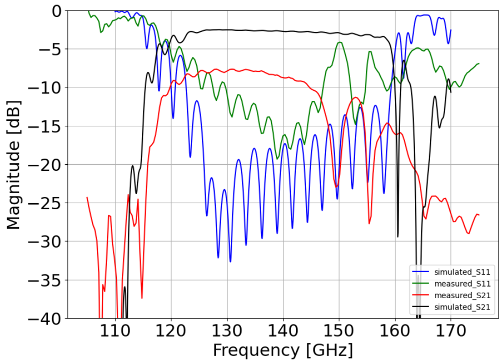

(b) $\lambda/4$ - Displaced by +100um

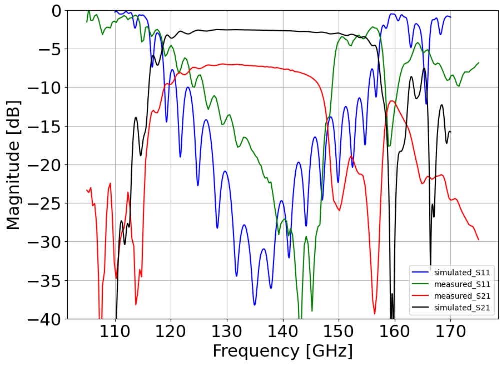

(c) $\lambda/4$ - Displaced by -50um

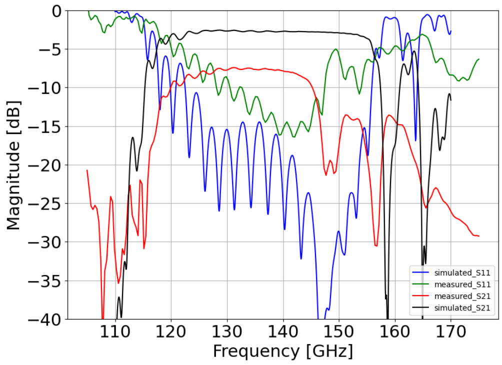

(d) $\lambda/4$ - Under etching by 10um

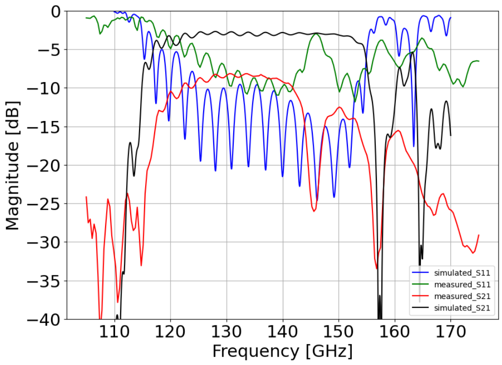

(e) $\lambda/4$ - Under etching by 20um

Figure A.4: Tolerance of simulated and measured results for quaterwave matching

DEPARTMENT OF SOME SUBJECT OR TECHNOLOGY
CHALMERS UNIVERSITY OF TECHNOLOGY
Gothenburg, Sweden
www.chalmers.se